This manuscript is a preprint and has been submitted to Tectonics. It has not undergone peer-review. Subsequent versions of this manuscript may have different content as a result of the review process.

Mesozoic drift of the Wrangellia superterrane revisited: the way forward from paleomagnetic data

Goran Andjić[1,2*], Bram Vaes[1], Suzanna H.A. van de Lagemaat[1], Lydian M. Boschman[1], Mark J. Dekkers[1], Stephen T. Johnston[3], and Douwe J.J. van Hinsbergen[1]

[1]*Department of Earth Sciences, Utrecht University, Princetonlaan 8A, 3584 CB Utrecht, the Netherlands*

[2]*Institute of Earth Sciences, University of Lausanne, Géopolis, 1015 Lausanne, Switzerland*

[3]*Department of Earth and Atmospheric Sciences, University of Alberta, Edmonton, AB T6G 2E3, Canada*

**Corresponding author: Goran Andjić (goran.andjic@unil.ch)*

Key Points:

- New and compiled paleomagnetic data from Mesozoic rocks of the Wrangellia superterrane show consistent inclinations and declinations
- Two new tectonic scenarios describe Wrangellia's drift from a Triassic subequatorial to a mid-Cretaceous, mid-latitude accreted position
- Robust and reproducible paleomagnetic data of Wrangellia are useful for solving the Baja-British Columbia controversy

Abstract

The allochthonous origin of the Wrangellia superterrane relative to North America has been established in the early days of plate tectonics using paleomagnetic and geological data. However, long-standing disagreement between paleomagnetic and structural studies on magnitude of northward translation of the Wrangellia superterrane during the Latest Cretaceous–earliest Cenozoic has cast doubt on the validity of the paleomagnetic data of the superterrane, including data from Paleozoic and Mesozoic rocks. Here, we compile all paleomagnetic data from the superterrane and present new results from uppermost Triassic limestones and lowermost Jurassic lavas of the Bonanza arc, which confirm that the Wrangellia superterrane was at those times at a much lower latitude than today, either ~25–35° North or ~25–35° South. Moreover, declinations reveal a coherent, major clockwise or counterclockwise rotation, depending on hemispheric origin. When correcting for previously documented true polar wander–the wholesale rotation of the solid Earth relative to the Earth's spin axis–at the approximate longitude of the Wrangellia superterrane, new and existing paleomagnetic data allows for two possible scenarios of Mesozoic kinematic evolution: from 190 Ma to 80 Ma, the Wrangellia superterrane was either transported ~5000 km northward while rotating ~110° clockwise at a north-dipping subduction zone or remained at northern middle latitudes while rotating ~70° counterclockwise at a south-dipping subduction zone. The robust and reproducible Triassic–lowermost Jurassic and Cretaceous paleomagnetic data make previously speculated systematic artifacts unlikely solutions for the kinematic debate on the Late Cretaceous to Eocene tectonic history of the Wrangellia superterrane.

1. Introduction

The Cordilleran orogen of northwestern North America is among the largest accretionary orogenic complexes that formed since Mesozoic time. The orogen developed at a series of subduction zones that collectively accommodated plate convergence between the Farallon and other oceanic Panthalassa plates, and the continental North America Plate (Engebretson et al., 1985; Nokleberg et al., 2000; Sigloch & Mihalynuk, 2013; van der Meer et al., 2012). Kinematic reconstruction of the Cordilleran orogen of North America is important for connecting surface geological processes to mantle dynamics (Sigloch & Mihalynuk, 2017; van der Meer et al., 2010, 2012), exploring economic resources (Nokleberg et al., 2005), and modelling the Earth's paleogeography (Scotese, 2021) and paleoclimate (Caruthers et al., 2021; Dal Corso et al., 2020). Restoring the kinematic history of the Cordilleran orogen requires quantifying the amount, timing, and direction of past displacement of the fault-bounded crustal fragments that compose the orogen. This appears at first glance straightforward: the Cordilleran orogen exposes terranes that sutured against the North American margin in the Mesozoic, and that were transported northward since Late Cretaceous times along margin-parallel strike-slip faults, accommodated by complex deformation and oroclinal bending in Alaska (e.g., Johnston, 2001). Such northward motions may be quantified from paleomagnetic data demonstrating paleolatitudinal motions, and structural estimates from fault displacements. However, this led to a long-standing, and unsolved problem: terrane displacements deduced from paleomagnetic data are much larger than those obtained from structural data on faults that quantify relative displacements between exposed rock units (Gabrielse et al., 2006).

The paleomagnetic point of view has been summarized as the Baja-British Columbia (Baja-BC) hypothesis. Paleomagnetic data from the western terrane of the Cordilleran orogen that currently makes up much of British Columbia–the so-called Wrangellia superterrane–were during the Late Cretaceous (~80 Ma) at the same latitude as Baja California (~30°N), implying a ~2000 km northward motion since the Late Cretaceous (Irving, 1985; Umhoefer, 1987). Field-based, structural geological correlations, however, so far cannot account for more than 800 km of displacement since that time (Gabrielse et al., 2006). If the conceptual solution is to be found in the geological estimates, a plate boundary-scale fault has remained unrecognized in the geological record (e.g., Cowan et al., 1997; Johnston, 2008). If the solution lies in the estimate of paleolatitude based on paleomagnetic data, then the Wrangellia superterrane should have suffered from a systematic, previously unrecognized regional paleomagnetic bias–such as tectonically induced remagnetization of igneous and sedimentary rocks and inclination flattening of sedimentary rocks unaccounted for (Butler et al., 2001b)–or there may have been flaws in the statistical procedures or the reference apparent polar wander path that constrains the paleolatitudinal position of North America (e.g., Kent & Irving, 2010; Torsvik et al., 2012). Finally, the use of paleomagnetic data obtained from intrusive rocks (e.g., Beck & Noson, 1972; Rusmore et al., 2013), from which interpretation is complicated by lack of control on paleohorizontal at the time of magnetization, has cast further doubt on the pertinence of using paleomagnetic data to quantify the northward transport of segments of the North American Cordillera (Butler et al., 2001b).

In this paper, we aim to re-assess the coherence and consistency of paleomagnetic data from the Wrangellia superterrane, and whether a paleomagnetic artifact or misinterpretation may lie at the heart of the Baja-BC problem. We therefore compile paleomagnetic data from the Wrangellia superterrane, which has a long history that predates the Upper Cretaceous: paleomagnetic data are available from rocks dating back to the early Paleozoic. The basement of the Wrangellia superterrane consists of a continental arc basement and sedimentary rocks that are overlain by a thick pile of Triassic lavas interpreted as a large igneous province, which is in turn overlain by the Late Triassic to Middle Jurassic “Bonanza” arc (Nokleberg et al., 2000). East, north, and south of the Wrangellia superterrane are the Intermontane terrane of the Canadian Cordillera and the Franciscan accretionary prism of Oregon and California, respectively, which both formed as part of the North American margin and consist of metamorphosed continental margin rocks, ophiolites, and accreted complexes that were amalgamated in a subduction zone between the Wrangellia superterrane and the North American continent since the Early Jurassic (Nokleberg et al., 2000; Wakabayashi, 2015). The Wrangellia superterrane is therefore thought to have been located in an upper plate position relative to a subduction zone that formed the Bonanza arc, but in a downgoing plate position relative to North America, until its collision with North America, sometime in the middle to Late Cretaceous (Nokleberg et al., 1994, 2000; Plafker et al., 1989; Tikoff et al., 2023). Such a Mesozoic double subduction system is consistent with slab remains imaged by seismic tomography that revealed parallel belts of mid-mantle slabs below western North America and the eastern Pacific (Clennett et al., 2020; Fuston & Wu, 2021; Sigloch & Mihalynuk, 2013, 2017; Sigloch et al., 2008; van der Meer et al., 2010, 2012, 2018). The extensive rock records of the Wrangellia superterrane dating back to the Paleozoic thus provides the opportunity to constrain the paleolatitudinal and rotational components of the pre-collisional plate motion history relative to North America.

Interestingly, paleomagnetic data from middle Paleozoic to Lower Jurassic (~450–180 Ma) rocks of the Wrangellia superterrane show that it was in a subequatorial position at these times (~0–25°; Bazard et al., 1995; Irving & Yole, 1987; Kent & Irving, 2010; and references therein), whereby northern and southern hemisphere options are both possible (Panuska & Stone, 1981). Both options suggest significant northward motion in the ~190–80 Ma interval, preceding the controversial Baja-BC problem. In this study, we compiled all paleomagnetic data from the Wrangellia superterrane, covering the Paleozoic to Cenozoic, and collected a new, large paleomagnetic dataset from uppermost Triassic sedimentary rocks and Lower Jurassic Bonanza arc lavas of the southern Wrangellia superterrane. We use these to test the reproducibility of paleomagnetic data from the youngest Mesozoic age interval for which previous data revealed a subequatorial position. We compare these data to an updated global apparent polar wander path (APWP; Vaes et al., 2023) and use data comparison methods (Vaes et al., 2021, 2022) that overcome statistical issues of classic paleomagnetic approaches (Rowley, 2019).

Not only do we test whether the inclinations, constraining paleolatitudinal position through time, provide a coherent pattern, but we also evaluate whether the declinations, constraining vertical axis rotations, provide a coherent history. We test rates of reconstructed northward motion of the Wrangellia superterrane against recent reconstructions of minimum oblique subduction components obtained from kinematic evidence from the Californian forearc ophiolites (Arkula et al., 2023), and from Ocean Plate Stratigraphy (OPS) accreted in the Californian Franciscan subduction complex (Alvarez et al., 1980; Courtillot et al., 1985; Tarduno et al., 1985, 1986). Finally, we evaluate whether reconstructed positions of the Bonanza arc at the time of the end of subduction coincide with the presence of slab remnants in mantle tomography. The updated statistical paleomagnetic procedures and reference frame, as well as the multiple independent tests, will determine whether paleomagnetic artifacts lie at the heart of the Baja-BC problem, allowing us to propose ways forward in reconciling paleomagnetic and structural data.

2. Geological context

2.1. The Wrangellia superterrane

From western Alaska to southeastern British Columbia, the Wrangellia superterrane is subdivided into the Peninsular, Wrangellia, and Alexander terranes (Figure 1a), which overall share a multi-stage history of arc magmatism that spans the Late Paleozoic and most of the Mesozoic (~360–100 Ma; Alberts et al., 2021; Nokleberg et al., 1994; Plafker & Berg, 1994). The amalgamation of the three terranes is thought to have occurred during the Paleozoic, prior to their Mesozoic accretion to North America. Below, we summarize the main geological features of each terrane and key moments in their tectonic evolution.

The core of the Wrangellia superterrane is the Alexander terrane, which is interpreted as a microcontinental fragment that was intruded by late Neoproterozoic to early Paleozoic arc-related rocks (~600–400 Ma; Gehrels & Saleeby, 1987; White et al., 2016). Volcanic and plutonic rocks dominate the southern part of the Alexander terrane, whereas the northern part consists mainly of Paleozoic shelf strata as old as the upper Cambrian (Beranek et al., 2012). Magmatic activity in the Alexander terrane was interrupted during two orogenic events, the Cambrian Wales orogeny and the lowermost Devonian Klakas orogeny (Gehrels & Saleeby, 1987).

The Alexander terrane is bordered to the south and the north by the younger Wrangellia terrane, which consists mainly of upper Devonian to lower Permian and upper Triassic to middle Cretaceous arc-related igneous and sedimentary rocks (Alberts et al., 2021; Nokleberg et al., 1994; Plafker & Berg, 1994). Although basement rocks underlying the Paleozoic arc have not been observed, detrital zircon data from the southern Wrangellia terrane suggest that it incorporated fragments of the Alexander terrane (Alberts et al., 2021). Geological ties between the Alexander and Wrangellia terranes dating back as early as ~360 Ma (Late Devonian) are corroborated by coeval gabbro complexes intruding both terranes (Israel et al., 2014).

An episode of plume-related volcanism occurred between the Paleozoic and Mesozoic arc phases of the Wrangellia terrane, forming the up to 6 km-thick Wrangellia large igneous province (Upper Triassic, ~232–226 Ma; Greene et al., 2010), which spans the whole length of the Wrangellia terrane. In our study area on Vancouver Island, the Bonanza arc was built on these flood basalts and associated sedimentary rocks (Canil et al., 2010, 2013; DeBari et al., 1999; D'Souza et al., 2016). The Bonanza Group consists here of a basal Upper Triassic–lowermost Jurassic volcanic-sedimentary succession (Parson Bay Formation and Volcaniclastic-Sedimentary unit; ~226–200 Ma, based on detrital zircon U-Pb geochronology and biostratigraphy) overlain by the Lower Jurassic Le Mare Lake Volcanic Unit (~201–190 Ma, based on zircon U-Pb geochronology and biostratigraphy) and the Lower to Middle Jurassic Holberg Volcanic Unit (~201–164 Ma, based on detrital zircon U-Pb and amphibole Ar-Ar geochronology; Nixon & Orr, 2007; Nixon et al., 2011a, 2011b, 2011c, 2011d). The latter volcanic units are interbedded with minor marine and non-marine epiclastic rocks and limestone. The bulk of the Bonanza arc complex was intruded by the Lower to Middle Jurassic Island Plutonic Suite (~201–164 Ma, based on zircon U-Pb and amphibole Ar-Ar geochronology; D'Souza et al., 2016; Nixon et al., 2011a, 2011b, 2011c, 2011d). The Le Mare Lake Volcanic Unit and the Island Plutonic Suite represent the main phase of growth of the Bonanza arc. On Vancouver Island, Triassic and younger units have experienced burial metamorphism to zeolite and prehnite-pumpellyite facies, implying temperatures below 350°C and pressures below 2.5 kbar (<10 km depth; Kuniyoshi & Liou, 1976; Lei et al., 2020; Morris & Canil, 2021; Stewart & Page, 1974).

Except for the absence of flood basalts, the stratigraphic architecture of the Peninsular terrane is similar to that of the Wrangellia terrane (Figure 1). The Peninsular terrane mainly consists of Upper Triassic to Middle Jurassic volcanic, plutonic, and volcaniclastic rocks of the

Talkeetna arc, overlain by Upper Jurassic to Lower Cretaceous volcaniclastic basinal strata (McClelland et al., 1992; Plafker et al., 1989; Rioux et al., 2007, 2010). The Talkeetna arc, considered as an archetypal intraoceanic arc, is lithologically, temporally, and geochemically correlative to the Bonanza arc of the Wrangellia terrane (D'Souza et al., 2016; Plafker et al., 1989; Rioux et al., 2007). Scarce outcrops of metamorphosed upper Paleozoic mafic to intermediate volcanic rocks, limestones, and quartz-rich sedimentary rocks provide a glimpse into the basement of the Talkeetna arc (Plafker et al., 1989). Zircon xenocrysts from the Talkeetna arc and younger volcanic products suggest ties with the Alexander and Wrangellia terranes from at least the early Carboniferous (~310 Ma; Amato et al., 2007; Bacon et al., 2012; Beranek et al., 2014).

Based on stratigraphic, structural, geochemical, and geochronological data from arc and accretionary complex rocks, the polarity of the subduction beneath the Wrangellia superterrane is thought to have been northward in western Alaska to eastward in British Columbia (in present-day coordinates) at least since ~ 200 Ma (Amato et al., 2013; Clift et al., 2005a, 2005b; Plafker & Berg, 1994; Trop & Ridgway, 2007). Notably, blueschist-facies metamorphic rocks were formed during the Early Jurassic in a subduction complex now juxtaposed against the seaward margin of the superterrane (Roeske et al., 1989; Sisson & Onstott, 1986).

The timing and latitude, and possible diachroneity of accretion of the Wrangellia superterrane to North America are not yet resolved. Basinal records in the suture zone between the northern Wrangellia superterrane and the Intermontane superterrane, which is located east of it, have been used to suggest timings of collision that include the Middle Jurassic (e.g., McClelland et al., 1992), the Late Jurassic (e.g., Trop & Ridgway, 2007), the Early Cretaceous (e.g., Hampton et al., 2010), the middle Cretaceous (e.g., Amato et al., 2013; Plafker et al., 1989), and the Late Cretaceous (e.g., Hults et al., 2013). Proponents of diachronous accretion suggest that the southern part of the Wrangellia superterrane in British Columbia collided during the Jurassic, whereas the northern part of the superterrane in Alaska collided during the Late Cretaceous (e.g., Manselle et al., 2020; Trop & Ridgway, 2007). These widely differing accretion scenarios mostly differ from each other in the amount of post-subduction translation that the Wrangellia superterrane experienced that has been interpreted based on paleomagnetic studies (Kent & Irving, 2010).

Notably, estimates of post-accretion translation of the superterrane based on detrital zircon data from northern Washington, southern British Columbia, and southern Alaska have not reached any consensus, with offsets ranging from ~500 km (Mahoney et al., 1999, 2021), through ~1000 km (Yokelson et al., 2015), to >1500 km (Boivin et al., 2022; Housen & Beck, 1999; Matthews et al., 2017; Sauer et al., 2019). Among these studies, the main disagreement revolves around the source of detrital zircons from the Upper Cretaceous Nanaimo Group of Vancouver Island, which may have been sourced from rocks outcropping in Idaho (~300–600 km south from Vancouver Island) and/or southern California (~1500–1800 km south from Vancouver Island; Boivin et al., 2022, and references therein). The latter option is compatible with paleomagnetic data from the Upper Cretaceous Nanaimo Group, which have consistently yielded paleolatitudes ~1600–2500 km south of its present-day location (Kim & Kodama, 2004; Krijgsman & Tauxe, 2006; Ward et al., 1997).

2.2. Jurassic ophiolites and OPS of California

Westernmost California and southern Oregon display a Mesozoic–Cenozoic subduction complex that formed by episodic accretion of Ocean Plate Stratigraphy (OPS), which records the history of a subducting oceanic plate from its formation to arrival at the trench (Isozaki et al., 1990). This subduction complex–the Franciscan Complex–accreted below Middle to Upper Jurassic (~170–155 Ma) supra-subduction zone ophiolites that are preserved as isolated klippen (Wakabayashi, 2015). The oldest accreted rocks are high-temperature, high-pressure metabasites interpreted as metamorphic sole rocks with Lu/Hf garnet ages of 180 Ma that mark the (minimum) age of subduction initiation (Mulcahy et al., 2018) and show that the ophiolites formed above an active subduction zone (e.g., Guilmette et al., 2018), consistent with their geochemical composition (Snortum & Day, 2020). Arkula et al. (2023) reconstructed western North American deformation to restore the relative positions of the Californian ophiolites in the Jurassic. They also showed paleomagnetic results that imply that the forearc paleo-ridges that generated the Jurassic ophiolites had near-perpendicular orientations to that of the Franciscan subduction zone. The kinematic restoration of the ophiolite belt shows that the paleo-ridges may have accommodated spreading rates of ~6 cm/yr, suggesting that the plate subducting obliquely beneath California in the Jurassic had a northward motion relative to North America of up to ~6–7 cm/yr.

The Franciscan Complex consists of rocks accreted from oceanic crust that formed since the Early Jurassic (Wakabayashi, 2015). The youngest accretion may have happened as recently as 12 Ma (McLaughlin et al., 1982). Among the accreted rock assemblages, two localities with middle Cretaceous limestone blocks provided paleomagnetic results that allow computing a paleolatitudinal journey of the OPS prior to accretion. The Laytonville limestone (103–90 Ma) yielded paleolatitudes of 17° ± 7° (Alvarez et al., 1980) and 14° ± 5° (Tarduno et al., 1986). The Calera limestone (129–90 Ma), located ~300 km southeast of Laytonville, yielded paleolatitudes of 24° ± 4° (Courtillot et al., 1985) and 18–25° at 105–90 Ma (Tarduno et al., 1985). Because the blocks may have rotated during accretion to the Franciscan Complex, it is not obvious whether they formed on the southern or northern hemisphere. Also, the accretion age of the limestone blocks to the Franciscan Complex has uncertainties. All scenarios show that in Early to Late Cretaceous times, the OPS sequences that accreted to the Franciscan Complex were derived from lower latitudes, moving north at rates varying from ~8 cm/yr for the northern hemisphere options (Courtillot et al., 1985; Tarduno et al., 1985) to ≥ 15 cm/yr for the southern hemisphere options (Alvarez et al., 1980; Tarduno et al. 1986). Additionally, OPS sequences with ages ranging from 180 to 110 Ma in the Santa Elena complex–part of the Chortis block that was connected to the North American continent (Andjić et al., 2019)–of western Costa Rica which accreted around 100 Ma at 11°N yielded paleolatitudes of 8-20° north or south (Boschman et al., 2021a).

3. Paleomagnetic sampling and measurements

To test the robustness of the paleomagnetic data from the youngest pre-Cretaceous rocks of the Wrangellia superterrane, we collected a total of 295 cores for paleomagnetic analysis from four localities in the Bonanza Group of northern Vancouver Island, Canada (Figure 2; Nixon et al., 2011a, 2011d). Locality YM ("Yreka Main") was sampled in a continuous ~50 m section of impure limestones of the Norian–Rhaetian Parson Bay Formation, from which 119 samples were collected (average dip direction = 230°, average dip = 50°, n = 8). Basaltic to andesitic lava flows of the Hettangian–Sinemurian Le Mare Lake Volcanic Unit were sampled in three sections (MD = "Main Drive", TT = "Teeta Creek", VL = "Victoria Lake") that are ~5 km apart, with each section consisting of ~15 m (TT: average dip direction = 226°, average dip = 38°, n=3) to ~50 m (MD: average dip direction = 273°, average dip = 29°, n = 14 ; VL: average dip direction = 196°, average dip = 33°, n = 12) of lavas. We used a gasoline-powered motor drill to sample 2.5 cm-diameter paleomagnetic cores, the orientation of which was measured with a magnetic compass with an inclinometer attached. We followed procedures recommended by Gerritsen et al. (2022) and drilled one core per limestone bed or volcanic flow (Figure S1 in Supporting Information S1) to optimize the amount of individual spot readings of the magnetic field, and as a field test selected a total of seven lava sites where 5 cores per lava flow were drilled to evaluate whether within-site scatter of paleomagnetic data is low (i.e., k values typically exceeding 50; e.g., Johnson et al., 2008). Measurements were corrected for the local declination (16°47' E to 16°48' E).

The cores were processed at the Paleomagnetic Laboratory Fort Hoofddijk at Utrecht University, The Netherlands. The cores were cut into 2.2 cm-long samples using a double-blade circular saw. To determine the nature of magnetic carriers for both types of sampled lithology (lavas and impure limestones), thermomagnetic analyses were performed using a horizontal translation-type Curie balance with a sinusoidally cycling applied magnetic field, usually 100–300 mT (Mullender et al., 1993). Several heating-cooling cycles were applied to detect magneto-mineralogical alterations during heating. We used the following temperature scheme (in °C): 150, 75, 225, 150, 300, 225, 375, 300, 450, 375, 525, 450, 600, 20 (for lavas); 250, 150, 350, 250, 450, 350, 520, 420, 620, 500, 700, 20 (for limestones). Stepwise thermal (TH) demagnetization was applied to 117 limestone samples and 30 lava samples, whereas stepwise alternating field (AF) demagnetization was applied to 72 limestone samples and 174 lava samples, the latter processed with a robotized magnetometer (Mullender et al., 2016). Natural remanent magnetizations (NRM) were measured on a 2G DC SQUID magnetometer. Temperature steps of 100, 180, 210, 240, 270, 300, 320, 340, 360, 380, and 400°C were used for TH treatment of 87 limestone samples. Temperature steps of 100, 180, 210, 240, 270, 300, 330, 360, 390, 420, 450, 480, and 510°C were used for TH treatment of 30 other limestone samples. Temperature steps of 100, 180, 210, 240, 270, 300, 330, 360, 390, 420, 450, 480, 510, 540, 570, and 600°C were used for TH treatment of the 30 lava samples. Demagnetization steps of 5, 10, 15, 20, 25, 30, 35, 40, 45, 50, 60, 70, 80, 90, 100, and 120 mT were used for AF treatment of all samples. To improve the resolution of AF demagnetization results of limestones, the latter were heated to 150°C in a thermal demagnetizer prior to AF treatments (van Velzen & Zijderveld, 1995).

Sample interpretation and statistical analysis were conducted using the online portal Paleomagnetism.org (Koymans et al., 2016, 2020). All results can be imported into the portal from data files (.col) available in the Supporting Information (Data Sets S1 and S2), as well as in the Paleomagnetism.org 2.0 database (Koymans et al., 2020) and the MagIC database (Jarboe et al., 2012). Demagnetization diagrams were plotted on orthogonal vector diagrams (Zijderveld, 1967), and the magnetic components were determined through principal component analysis (Kirschvink, 1980). Great circle solutions were determined using the method of McFadden and McElhinny (1988). The fold test (Tauxe & Watson, 1994) and the bootstrapped coordinate reversal test (Tauxe, 2010) were used when applicable. The elongation-inclination (E/I) correction for inclination shallowing (Tauxe & Kent, 2004; Tauxe et al., 2008) was applied to the sedimentary locality, but its result was not used in our interpretations, as discussed in section 4.2. A maximum angular deviation cut off (i.e., MAD ≤ 15°) was not applied to our dataset because it only reduces the number of samples, which decreases paleopole precision (Gerritsen et al., 2022). Paleomagnetic pole positions were calculated using Fisher (1953) statistics on virtual geomagnetic poles (VGPs)–whereby each VGP is derived from a single site–following statistical procedures described in Deenen et al. (2011), providing a measure of the VGP dispersion (Fisher precision parameter, K) and a 95% confidence ellipse on the pole position (A_{95}). The mean paleomagnetic direction and the 95% confidence regions on the declination (ΔD_x) and inclination (ΔI_x) were computed from the paleomagnetic pole and its A_{95}. A 45° cutoff was applied to the VGPs (Johnson et al., 2008) at the group level for the volcanic localities (TT, MD, VL). We did not apply this cutoff to the sedimentary dataset (YM), as that the application of this cutoff would not lead to the exclusion of any of the data points.

4. Results

4.1. Volcanic rocks (samples VL-TT-MD)

Thermomagnetic curves show that lava samples have Curie temperatures close to 580°C (Figure 3), indicating that magnetite is the main magnetic carrier. In orthogonal vector plots, the majority of the VL (58/80) and MD (32/54) samples reveal an overprint at low temperature/coercivity steps (up to ~100–240 °C or 5–15 mT). VL samples (46/80) have an additional overprint at mid-range temperature/coercivity steps (~420–570°C or 15–90 mT), most of which (40/46) did not yield characteristic remanent magnetization (ChRM) directions. In contrast, TT samples show a linear decay towards the origin of demagnetization diagrams without overprints. Initial intensities ranged 7–550 mA/m for TT, 0.2–38 mA/m for MD, and 0.6–1650 mA/m for VL. ChRM values were generally interpreted between 420–570°C or 10–120 mT for TT, ~270–510°C or ~25–70 mT for MD, and ~240–510 °C or ~20–70 mT for VL. Interpreted ChRM directions from most samples yielded eastward declinations with shallow upward inclinations (in tilt-corrected coordinates; Figure 3); one TT sample and ten MD samples yielded westward, down directions that suggest opposite polarity. Which of these two directions represent normal or reversed is not a priori known, and depends on the hemisphere of origin. Opposite-polarity ChRM directions of locality MD share a common true mean direction (CTMD); reversals are located throughout the section at samples MD1.9, MD1.23, MD1.24, and MD1.39–MD1.44. Mild differences in bedding orientation among the three localities were used for a regional fold test, but bedding differences are insufficient to yield a conclusive result (best clustering between 59 and 78% unfolding).

The lava sites from which we collected multiple samples per site returned low dispersion results (e.g., k = 395.9 for TT 1.31–1.35 and k = 54.8 for MD 1.16–1.2; Figure 3), confirming that lava sites may be treated as spot readings of the field. The paleomagnetic pole computed from the lava sites is located at latitude = 35.0°S, longitude = 340.8°E (N = 117, K = 18.0, A_{95} = 3.2°), corresponding to a paleomagnetic direction of *Declination (D)* ± ΔD_x = 102.6° ± 3.9°, *Inclination (I)* ± ΔI_x = -54.2° ± 3.2° (Figure 3, Table 1). The D and I values of the combined volcanic localities differ significantly from the recent GAD field (D/I = 000°/70°). The A_{95} value (A_{95min} = 1.8° < A_{95} = 3.2° < A_{95max} = 4.1°) satisfies the N-dependent reliability envelope of Deenen et al. (2011), suggesting that the observed VGP scatter can be straightforwardly explained by paleosecular variation (PSV).

4.2. Sedimentary rocks (samples YM)

Thermomagnetic curves of the limestones show two types of magnetic carriers. Samples YM 1.91 and YM 1.118 have very low initial magnetization, even diamagnetic, i.e., the signal is dominated by the quartz glass sample holder. The curves are completely reversible after cycling to 250°C and show minor decay after the 350°C cycle, with a pyrite-to-magnetite oxidation signature developing after 420°C (e.g., Passier et al., 2001). On cooling to room temperature after the 700°C cycle, a discontinuity at ~320°C is observed, the Curie temperature of pyrrhotite (Figure 4 and Figure S2). In contrast, samples YM 1.52 and YM 1.61 present a much higher (~50–100 times) initial magnetization, with smooth curves that are essentially reversible up to 500°C, which supports the presence of titanomagnetite with a variable Ti content (Figure 4 and Figure S2). Interestingly, both groups of samples have similar values of their initial NRM (YM 1.52 = 3.3 mA/m, YM 1.61 = 4.1 mA/m vs. YM 1.91 = 6.0 mA/m, YM 1.118 = 5.1 mA/m), which suggests that the efficiency of the NRM acquisition mechanism differs widely between the two groups. YM1.91 and YM1.118 feature a chemical remanent magnetization (CRM) which is an efficient NRM acquisition mechanism while the NRM of YM1.52 and YM1.61 is much less efficient (a lot more magnetic material is required for a similar NRM intensity) which would imply a detrital remanent magnetization (DRM). Nonetheless, after thermal demagnetization at 360°C, usually <10–15% of the initial NRM intensity remains for both types of samples. This implies that ChRM directions were interpreted from the same temperature steps for both groups.

Initial NRM intensities ranged 0.3–115 mA/m, with values mostly restricted to 2–6 mA/m for samples from which ChRMs were interpreted. In orthogonal vector plots, magnetic components could not be determined from a subset of samples (49/189) because of erratic demagnetization behavior. The maximum applicable alternating field (120 mT) was not high enough to fully demagnetize limestone samples with AF demagnetization. Nevertheless, ChRM directions interpreted from AF demagnetization diagrams agree well with those obtained from TH demagnetization diagrams. A few samples (5/140) show an overprint at low temperature/coercivity steps (~100–210 °C or 5–20 mT). ChRM values were generally interpreted at ~210–360 °C or ~30–70 mT, yielding down, westward directions. The paleomagnetic pole computed for locality YM is located at latitude = 23.0°N, longitude = 151.9°E (N = 138, K = 52.7, A_{95} =1.7°), providing a direction with $D \pm \Delta D_x$ = 278.1° ± 1.8°, $I \pm \Delta I_x$ = 40.2° ± 2.3° (Figure 4, Table 1). The D and I values of YM differ significantly from that of the recent GAD field (D/I = 000°/70°).

Overall, we find that the results of the YM limestones are consistent with them dominantly carrying a CRM, that was acquired soon after sediment deposition, and that resulted in ChRM acquisition that integrated secular variation over a longer duration, possibly over $\geq 10^3$ yr. This is compatible with the following aspects: (i) No polarity reversals have been measured in the YM limestones; (ii) The relatively low dispersion of the VGPs of the limestones yield an A_{95} that coincides with the A_{95min} of the reliability envelope of Deenen et al. (2011); (iii) After removing great circle solutions (n = 9) from the dataset (following Vaes et al., 2021), we performed the E/I correction of Tauxe and Kent (2004) using Paleomagnetism.org (Koymans et al., 2016, 2020), which yielded a flattening factor of 0.8 and a slightly higher inclination of 46.6° (95% bootstrapped confidence bounds of 41° to 62°; Figure S2). We note that the elongation of the YM directions (~1.68) is close to that predicted by the TK03.GAD field model (~1.78), which is compatible with a DRM contribution in a portion of the samples and/or CRM acquisition during (early) diagenesis.

4.3. Summary of the results

There is no independent control on the hemispheric origin and direction of rotation (clockwise or counterclockwise) for the YM and combined MD–TT–VL localities, since both normal and reversed polarities are common in the Norian–Rhaetian and Hettangian–Sinemurian, respectively. Therefore, for each paleomagnetic dataset, there are two possible solutions corresponding to either the northern or southern hemisphere, with opposite directions of rotation. The northern hemisphere option for the sediment-derived dataset (YM) yields a paleolatitude of 22.9° ± 1.7° N and a ~82° counterclockwise rotation, whereas the southern hemisphere option yields a paleolatitude of 22.9° ± 1.7° S and a ~98° clockwise rotation. The combined result of the igneous localities of the Bonanza Group (MD-TT-VL) yields a northern hemisphere solution with an estimated paleolatitude of 34.7° ± 3.2° N and a ~77° counterclockwise rotation, with a southern hemisphere solution providing a paleolatitude of 34.7° ± 3.2° S and a ~103° clockwise rotation.

5. Updated paleomagnetic database for the Wrangellia superterrane

We combine our new data with a database of available paleomagnetic data from the Wrangellia superterrane that we compiled from the literature. We only chose data from the NW-SE striking part of the Wrangellia superterrane, from southern British Columbia to eastern Alaska, and left the western and northern parts of Alaska out of the compilation, as these were likely strongly rotated in Late Cretaceous to Paleocene times during oroclinal bending (Johnston, 2001). Our database includes datasets that contain at least eight individual directions of the magnetic field (either from eight individual cooling units in magmatic rocks, or eight sedimentary beds, as suggested by Meert et al., 2020), and of which the distribution of magnetic directions passes the Deenen et al. (2011) criterium of representing paleosecular variation ($A_{95min} < A_{95} < A_{95max}$). We excluded datasets from the compilation when the authors of the original study interpreted the magnetic signal to represent a remagnetization (Hillhouse & Grommé, 1980; Irving & Massey, 1990; Symons, 1985), in cases in which rocks with an unknown paleohorizontal were sampled (Butler et al., 2001a; Irving et al., 1985; Irving & Massey, 1990; Rusmore et al., 2013; Symons, 1973), or in which shearing was interpreted to have influenced the magnetic directions (Butler et al., 2002).

Our compilation contains datasets for Early Jurassic and older times, and for Late Cretaceous and younger times. There are two small datasets from the Lower Cretaceous of Alaska that were collected by Stone et al. (1982), and some preliminary results provided by Panuska et al. (1984). However, the original data and descriptions are not available, and the datasets were considered unreliable by subsequent studies (Butler et al., 1997; Harbert, 1990; Hillhouse, 1987). In addition, Butler et al. (1997) revisited Ordovician, Silurian, Devonian, and Carboniferous rocks of the Wrangellia superterrane from which Van der Voo et al. (1980) reported paleolatitudes. Butler et al. (1997) argued that these Paleozoic rocks were remagnetized in the Triassic, and that none of these provide useful paleogeographic information. We show the data of Van der Voo et al. (1980) in our compilation but we consider them as potentially unreliable, as discussed further in section 6.1.

The final compilation consists of a total of 39 collections from 18 studies, 23 for the Late Cretaceous and younger, and 16 for pre-Late Cretaceous times (Figure 6; Tables S1 and S2 in Data Set S3). For Late Cretaceous and younger times, paleolatitudes are all ~30° or higher and interpreted as northern hemispheric. For the older datasets, paleolatitudes can be either southern or northern hemispheric, with the exception of rocks from the upper Carboniferous-Permian Kiaman superchron (~320–260 Ma; Opdyke & Channell, 1996), which must be reversed if they carry a primary magnetization. In Figure 6, we present both hemispheric options.

6. Discussion

6.1. Paleomagnetic data from the Wrangellia superterrane: primary or secondary magnetizations?

To evaluate the paleomagnetically permissible plate motions of the Wrangellia superterrane since the Triassic, we now use the updated paleomagnetic database, which includes our two new poles that are the largest paleomagnetic datasets for the Wrangellia superterrane to date and whereby our sediment-based dataset is corrected for inclination shallowing (except for our new sedimentary pole). First, we briefly re-evaluate whether the new global APWP of Vaes et al. (2023) for the last 320 Ma provides significant modifications to the paleolatitude and declination of the North American continent. This new path is based on directional paleomagnetic data rather than on compilations of paleomagnetic poles that were previously used (e.g., Kent and Irving, 2010; Torsvik et al., 2012; see Vaes et al., 2022, 2023, for details). As illustrated in Figure 5, the global APWP of Vaes et al. (2023) gives a smaller uncertainty but is mostly within error of previous APWPs (in North American coordinates). We compare the data of the Wrangellia superterrane with the APWP of Vaes et al. (2023) for the last 320 Ma, and with the moving average of Laurentia APWP of Torsvik et al. (2012) for earlier parts of the Paleozoic (Figure 5).

Plotting the database against a North American reference curve, in northern and southern hemisphere scenarios, allows us to re-evaluate previous hypotheses on the primary or secondary nature of paleomagnetic data. First, we note that both declinations and inclinations from Paleozoic to Lower Jurassic rocks of the Wrangellia superterrane are systematically different from those of the Upper Cretaceous to Cenozoic rocks. If a regional unrecognized remagnetization in Upper Cretaceous or younger time had occurred, creating apparently low paleolatitudes by erroneously correcting for bedding tilt (Butler et al. 2001b; Hollister et al., 2004; Housen & Beck, 1999; Monger & Price, 1996; Nelson & Colpron, 2007), then that remagnetization would also have affected older rocks. The coherent, systematically deviating paleomagnetic directions of pre-Upper Cretaceous rocks makes a regional remagnetization in Late Cretaceous or younger times unlikely.

On the other hand, previous arguments for remagnetization of Paleozoic rocks (Butler et al., 1997) cannot be excluded. Rocks older than the Triassic have declinations as well as inclinations that are similar to those from the Triassic Wrangellia large igneous province (Figure 6). If not remagnetized during the eruption of the large igneous province, these rocks would suggest that for a period of ~250 Ma, from the Devonian to the Triassic, Wrangellia was part of a plate that was not moving in paleolatitude much, nor undergoing systematic vertical-axis rotations. We therefore do not interpret the pre-Triassic history of Wrangellia here in detail. We note, however, that the northern hemisphere-counterclockwise rotation scenario permits that the Paleozoic data are primary, whereas the southern hemisphere, clockwise rotation scenario requires that at least the rocks from the Carboniferous-Permian Kiaman superchron do not carry a primary magnetization. Future detailed paleo- and rock magnetic study of these rocks may thus be helpful in evaluating the possibility of this scenario.

6.2 Paleomagnetic constraints on Wrangellia plate motion since the Triassic

When inspecting the paleomagnetic dataset of the Wrangellia superterrane, compared to the APWP of North America as reference, we first note that the two hemispheric options yield consistent declinations (Figure 6). These cluster in either ~100° clockwise or ~80° counterclockwise rotation relative to the magnetic north pole since the Early Jurassic. Previous workers have mostly focused on paleolatitudes and assumed that declinations were unreliable because of local rotations related to orogenic deformation (e.g., Kent & Irving, 2010). Such local rotations would of course be easily explained, given that the Cordilleran orogen has been folded, faulted, and transported northward along the North American margin, possibly along major strike-slip faults (Beck, 1976, 1980; Irving & Yole, 1987). However, inspection of the database does not suggest that local rotations play a major role. The scatter in declinations for collections of Upper Cretaceous rocks of the Wrangellia superterrane is several tens of degrees (Figure 6). Much of these data collections are small, based on a dozen or so datapoints (Tables S1 and S2 in Data Set S3). Even the datasets behind global APWPs, collected from stable plate interiors, are scattered over 30-40° mostly because of un-averaged paleosecular variation (Rowley, 2019; Vaes et al., 2022). The declination scatter of the Wrangellia superterrane is larger than that, suggesting that local tectonic rotations slightly enhanced it. Nonetheless, the declinations of Jurassic rocks are not chaotic: Lower Mesozoic and older rocks yield declinations that are systematically much larger than those of the Upper Cretaceous rocks, but their scatter is similar to the latter (Figure 6). We therefore infer that the Wrangellia superterrane underwent a coherent rotation between the Early Jurassic and the Late Cretaceous, i.e., during the pre-collisional period when it was part of a plate converging with North America. In a southern hemisphere scenario (Scenario S), this corresponds to a ~110° clockwise rotation relative to North America, whereas in a northern hemisphere scenario (Scenario N) it represents a counterclockwise rotation of ~70° (Figure 6).

Previous data from Triassic and older rocks of the Wrangellia superterrane yielded paleolatitudes close to the equator. Our new dataset shows a rapid paleolatitudinal motion on the order of 20-30° in the Late Triassic to Earliest Jurassic, which is northward in Scenario N, and southward in Scenario S (Figure 6). In Scenario S, this is followed by a northward motion of ~60° in ~120 Ma. In Scenario N, paleolatitudes would remain fairly constant until the Late Cretaceous.

To interpret what such paleolatitudinal drifts would mean for plate motion rates we compare these trajectories with the paleolatitudinal motion of North America. Moreover, it is important to note that the paleolatitude of North America is affected by a major phase of True

Polar Wander (TPW) that occurred in Late Triassic to Jurassic times (Steinberger & Torsvik, 2008; Torsvik et al., 2012; Vaes, 2023). Comparison between the global APWP of Vaes et al. (2023) with the recent mantle reference frame based on a series of tectonic 'rules' of Müller et al. (2012) suggested that the pole of TPW was in the Atlantic Ocean (Vaes, 2023), close to the earlier inferred pole based on the shared rotation of all plates in the paleomagnetic reference frame of Steinberger & Torsvik (2008). At the longitude of western North America, this TPW phase caused a southward and then northward shift in latitude on the order of 15° with a peak magnitude of TPW around 200 Ma. Farther west, in the eastern Panthalassa Ocean where the Wrangellia superterrane must have been, the magnitude of TPW increased up to a maximum of ~20°.

Scenario S gives a southward shift of the Wrangellia superterrane in the Triassic, followed by a northward motion. Much of this southward shift could be the result of TPW. Taking the TPW reconstruction of Torsvik et al. (2012) into account, approximately half of the southward latitude change of the Wrangellia superterrane between ~220 and 190 Ma may have been caused by TPW, suggesting ~10–15° absolute southward motion at subequatorial latitudes. Because Jurassic motion of North America was northward, northward motion of Wrangellia relative to North America was ~50° between ~190 and ~80 Ma ago, a period of 110 Ma (Figure 6). There are currently no high-quality paleomagnetic data to further specify how this relative northward motion was distributed through time.

Scenario N requires a rapid northward shift of ~20° of the Wrangellia superterrane in the Late Triassic to Earliest Jurassic. It is important to note that this motion is opposite to the TPW-induced southward motion, which means that the plate tectonic motion in Scenario N is larger, by about ~15°, than the paleomagnetically determined motion, followed by a net paleolatitudinal standstill until the Late Cretaceous. Because North America kept moving northwards in the Jurassic, this would require that the plate carrying the Wrangellia superterrane moved southwards relative to North America, i.e., with a left-lateral strike-slip component. Below, we place both scenarios in further plate tectonic context.

6.3. Wrangellia in context of eastern Panthalassa plate kinematic history

We now explore the plate tectonic consequences and feasibility of the paleomagnetic scenarios above. A detailed kinematic restoration of Cordilleran orogenic architecture is required to fully justify a final choice between the two options, which is beyond the scope of the current paper. We therefore restrict ourselves here to outlining the implications, solutions, and problems that the two scenarios generate.

We present a simplified reconstruction in Figure 7. The paleolatitudinal position of a simple, straight Wrangellia superterrane (which does not include the portions bent into Alaska; Johnston, 2001) relative to North America was determined in the paleomagnetic reference frame of Vaes et al. (2023), whereby we assumed a 190 Ma-position of ~30° south or north. Because we now aim to develop a plate tectonic scenario and compare it to seismic tomographic constraints, we placed the reconstruction in the TPW-corrected paleomagnetic reference frame of Torsvik et al. (2012). We note that this frame has no paleolongitudinal constraints, so we restrict ourselves in the comparison to tomography and latitudinal fits only.

The paleolongitudinal position of the Wrangellia superterrane relative to the Americas is not constrained by paleomagnetism, but options are restricted given the estimated position of the Farallon-Phoenix-Izanagi triple junction at which the Pacific Plate formed at 190 Ma (Boschman & van Hinsbergen, 2016). The position of this triple junction must have been located in the eastern Panthalassa Ocean to maintain convergence of the major Panthalassa plates with the surrounding continents, and we use the approximated position of Boschman et al. (2021a). This gives the Wrangellia superterrane a possible paleolongitudinal range of ~5000 km at 190 Ma.

From Late Triassic (~210 Ma) to Middle Jurassic times (165 Ma), when the Bonanza arc was active, the Wrangellia superterrane was in an upper plate position of a subduction zone. In present-day coordinates, the trench is thought to have been located to the west of the Wrangellia superterrane (Clift et al., 2005b; Trop & Ridgway, 2007). This means that in the southern hemisphere, clockwise rotation Scenario S, the Bonanza arc was underlain by a northward dipping subduction zone. In the northern hemisphere, counterclockwise rotating Scenario N, the arc was underlain by a southward dipping subduction zone.

We evaluate the scenarios against the evidence for oblique subduction below the California forearc between 170 and 160 Ma with a N-S component of ~6-7 cm/yr, concluded from reconstructing the Californian ophiolites (Arkula et al., 2023), and the evidence for a northward motion component throughout the Cretaceous suggested by the paleolatitudes of the accreted seamounts of the Franciscan accretionary complex of California (Courtillot et al., 1985; Tarduno et al., 1985, 1986). In addition, a northward motion component is also permitted in line with the OPS that accreted to the western margin of the Chortis block in the Early

Cretaceous, although a stable eastward relative plate motion is also permitted there (Boschman et al., 2021a).

We use two additional constraints in the 190–80 Ma time window to illustrate the implications of the two scenarios. First, the Caribbean Plate contains Jurassic crust that formed around ~160–150 Ma, and that was part of the Farallon Plate prior to the ~100 Ma onset of subduction at the western Caribbean subduction zone (Boschman et al., 2019). This crust likely formed at the Farallon-Phoenix spreading ridge, and paleomagnetic data reveals that this crust was located around the equator during the Late Jurassic (Boschman et al., 2019). This requires that by ~160 Ma, the Wrangellia superterrane must have been located to the north of the Caribbean lithosphere, and that it has likely always been located to the north of the Phoenix-Farallon spreading ridge.

Second, the Bonanza arc subduction must have been associated with a subducting slab, which likely broke off around or shortly after the time of arc cessation, ~165 Ma. Slabs may during their subduction be dragged horizontally through the mantle over 1000 km or more, driven by absolute plate motion of the subducting plate (Parsons et al., 2021; Qayyum et al., 2022; Spakman et al., 2018; van de Lagemaat et al., 2018), and the present-day position of the slab remains of the Bonanza arc subduction zone may no longer reflect the location at which subduction started. However, tomography-plate reconstruction correlations suggest that slabs undergo no major horizontal motion after their break-off (Domeier et al., 2016; van der Meer et al., 2010, 2018), which suggests that the Bonanza arc-related slab is likely located in the lower mantle beneath the location where it broke off. This slab is likely one of the western belt slabs that have been identified below and west of North America (Clennett et al., 2020; Sigloch & Mihalynuk, 2013, 2017; van der Meer et al., 2010, 2012). The southernmost of these, the Malpelo slab west of Colombia, was previously considered a candidate to be linked to the Bonanza arc (van der Meer et al., 2018), but because the Caribbean and western South American Jurassic to Lower Cretaceous arcs have been located at that paleolatitude (Boschman et al., 2019), these may provide a better candidate to explain the Malpelo slab. The southernmost slab of the western belt that cannot be explained by Caribbean arcs is the Socorro slab (van der Meer et al., 2010; 2018), at a latitude of ~15°N (Figure 1). It is also not likely that this slab correlates to subduction records of the Guerrero terrane (in Mexico), which was built since Triassic time on accretionary prism rocks formed at the North American margin and was only temporarily separated from North America by a short-lived and likely narrow back-arc basin (Boschman et al., 2018a, 2018b; Busby et al., 2023; Martini et al., 2014). Because the

Bonanza arc is the southernmost intra-oceanic arc complex in the Cordilleran orogen, we therefore discuss in our scenarios S and N whether this slab may have been linked to the Bonanza arc.

Both scenarios share the post-80 Ma history in which paleomagnetism places the Wrangellia superterrane approximately 20° south of its present latitude–the basis for the Baja-BC hypothesis that remains difficult to reconcile with structural geological correlations. The declinations are scattered and permit a rotated or a non-rotated position relative to today (Figure 6). In our schematic reconstructions, we place the Wrangellia superterrane in a non-rotated position, parallel to and close to the North American margin. We are well aware of the controversy around this reconstruction (e.g., Johnston, 2001; Trop & Ridgway, 2007), or even around the timing of the Wrangellia superterrane accretion (e.g., Gehrels et al., 2009; Hampton et al., 2010; McClelland et al., 1992; Monger, 2014; Nokleberg et al., 2000; Saleeby, 2000; Trop et al., 2002; Stevens Goddard et al., 2018; Tikoff et al., 2023), or diachroneity of accretion (e.g., Manselle et al., 2020; Nokleberg et al., 2000; Pavlis et al., 2019; Trop & Ridgway, 2007). At this stage, we have no satisfactory solution for where the northward motion that remains unaccounted for in the structural record was accommodated. The position of the Wrangellia superterrane in our simple reconstruction is based on paleolatitude only, and the general agreement that by 80 Ma, the Wrangellia superterrane was located along the North American margin. We note, however, that the ~190–80 Ma history discussed below, during which the northern or southern hemisphere options play a role, would not change if we assumed a more northerly position for the Wrangellia superterrane at 80 Ma.

Scenario N requires a few thousand kilometers of northward motion of the Wrangellia superterrane relative to the mantle in the Late Triassic–Early Jurassic, which with southward subduction requires roll-back of the slab below the Bonanza arc. Between 190 and 80 Ma, the Wrangellia superterrane remains at middle latitudes until its collision with North America, in which case the Bonanza arc was not associated with subduction of the Socorro slab. Another southward dipping subduction zone must therefore have existed between the Wrangellia superterrane and the Farallon Plate, which in Late Jurassic to Early Cretaceous time must have experienced a northward motion component (Arkula et al., 2023; Courtillot et al., 1985; Tarduno et al., 1985, 1986). Reconstructing the Wrangellia superterrane farther south around the mid-Jurassic, as depicted in Figure 7, would require slab advance of the Bonanza subduction zone, combined with another southward dipping subduction zone to accommodate the convergence between the Wrangellia superterrane and the Caribbean lithosphere which remained around equatorial latitudes (Boschman et al., 2019). Finally, the arrival of the Wrangellia superterrane at the North American margin must have involved a complex, counterclockwise plate rotation so that the western margin of the Wrangellia superterrane faced the Panthalassa Ocean. This counterclockwise rotation cannot be reconstructed without generating Farallon-Wrangellia convergence, requiring a syn-rotation, westward dipping subduction zone between these plates.

Scenario S also requires roll-back of the subduction zone below the Wrangellia superterrane in the Late Triassic–Earliest Jurassic, but southward, over ~15° latitude. This must have been followed by a northward shift over as much as 30° until the Middle Jurassic, by which time Caribbean lithosphere was forming to the south of the Wrangellia superterrane around the equator (Boschman et al., 2019). This northward Wrangellia motion occurred during activity of the Bonanza arc, and thus occurred during subduction. Hence, it must have been associated with slab advance and dragging over large distances. In Scenario S, it is possible that the Socorro slab represents the lithosphere that detached below the Bonanza arc upon its cessation in the Middle Jurassic. Following this cessation, northward motion of the Wrangellia superterrane continued while the plate carrying it rotated clockwise. This rotation is faster than that reconstructed for the Farallon Plate from Pacific anomalies (e.g., Seton et al., 2012), so it requires that the Wrangellia superterrane was part of a separate plate. However, no subduction zones are required between the Wrangellia superterrane and the Farallon Plate: its clockwise rotation could have been accommodated by subduction between the Wrangellia superterrane and North America, and the systematic northward motions are consistent with the paleomagnetic evidence from accreted OPS units (Courtillot et al., 1985; Tarduno et al., 1985, 1986) and North American upper plate ophiolites (Arkula et al., 2023). Subduction reactivation west of the Wrangellia superterrane is only required upon its accretion to North America (and may thus serve as a constraint on collision age).

6.4 The way forward

The two scenarios discussed above satisfy paleomagnetic constraints and illustrate the complexity in reconstructing the plate kinematic history of the northeastern Panthalassa Ocean. We consider it premature to make a firm choice between the northern and southern scenarios, but our analysis shows possible ways forward. First, our analysis shows that paleomagnetic data provide coherent and consistent results, not only in paleolatitude but also in declination.

A key step forward is filling the paleomagnetic data gap for the Wrangellia superterrane in the Late Jurassic and Early Cretaceous. Second, advances have been made in reconstruction of lost lithosphere of the Panthalassa Ocean and the Caribbean regions back to Jurassic times and before from geological records of accretionary prisms (Boschman et al., 2019, 2021a, 2021b; van de Lagemaat et al., 2023; Wright et al., 2016). Third, the rich seismic tomographic imagery of the upper and lower mantle below the former northeastern Panthalassa Ocean demonstrates where remains of subduction are currently residing (Sigloch & Mihalynuk, 2013; Sigloch et al., 2008; van der Meer et al., 2010, 2012). Reconstructions using those tomographic images as evidence for plate kinematic evolution has so far not led to reconstructions that also satisfy geological observations from the Cordillera of North America (Pavlis et al., 2019, 2020; Sigloch & Mihalynuk, 2020), but slab remnants may be helpful in determining where subduction terminated in the geological past. We foresee that a holistic analysis of geological architecture of the Cordillera, in which paleomagnetic constraints and seismic tomographic analyses are cast in context of Panthalassa and western ‘Pangean’ plate reconstructions, providing kinematically feasible scenarios. Those scenarios may serve to identify the key assumptions and interpretations that underpin the long-lasting controversy of Wrangellia’s motion history relative to North America, both before and after collision. Solving this controversy is important, because the error (or errors) which must exist in our thinking of tectonics or paleomagnetism, or both, are difficult to find and identifying them may provide fundamental lessons with repercussions in orogenic and plate reconstructions elsewhere.

7. Conclusions

Based essentially on paleomagnetic constraints, the Wrangellia superterrane is widely thought to have been located in an intraoceanic setting during most of the Mesozoic. In this study, we show that new and previous Triassic to Lower Jurassic paleomagnetic data of the Wrangellia superterrane are coherent in terms of inclination and declination throughout a 2000 km-long stretch of the superterrane that lies south of the Alaskan orocline. To address the hemispheric ambiguity of these paleomagnetic data, we propose two scenarios in which the Wrangellia superterrane was located either in the southern hemisphere (Scenario S) or in the northern hemisphere (Scenario N) at ~190 Ma. From ~190 to 80 Ma, the Wrangellia superterrane moved northward while rotating 110° clockwise at a north-dipping subduction zone (Scenario S) or remained at northern middle latitudes while rotating 70° counterclockwise at a south-dipping subduction zone (Scenario N). The main conclusion that can be drawn from comparing these scenarios is that scenario S represents the simplest solution to transport the Wrangellia superterrane from the equator to a position alongside North America allowing its accretion after a significant (clockwise) rotation. In contrast, scenario N requires at least two additional steps in the overall motion of the Wrangellia superterrane towards North America: (1) after a rapid northward shift of ~20° in the Late Triassic to Earliest Jurassic, the superterrane moved southward during the Early Jurassic; (2) the superterrane rotated away from North America during the Middle Jurassic before moving eastward to be accreted to North America. Although new paleomagnetic data from Early Cretaceous rocks are required to test both scenarios, the clockwise rotation in Scenario S fits existing models of Early Cretaceous paleogeography in which the Wrangellia superterrane accreted to the Intermontane superterrane through a northward zipper closure of the ocean between them.

In both scenarios N and S, the accretion of the Wrangellia superterrane to the Intermontane superterrane must have taken place >1500 km south of their present location. Interestingly, Upper Cretaceous to lower Cenozoic paleomagnetic data suggest a common northward motion of the amalgamated Wrangellia and Intermontane superterranes from ~35°N (at ~70 Ma) to ~50°N (at ~50 Ma), which is at odds with the estimates of northward motion (<800 km) obtained from major strike-slip faults located east of the Intermontane superterrane. By combining Triassic to Cretaceous paleomagnetic data with geological constraints on subduction polarity and mantle tomography, we found that Late Cretaceous paleomagnetic data yielding middle latitudes (~35°N) should not be discarded when reconstructing the tectonic history of the Wrangellia superterrane. Overcoming the fact that paleomagnetic and structural datasets yield apparently robust, yet contradicting estimates of northward motion of the Wrangellia superterrane will require enhanced collaboration across disciplinary specialties. In future studies, to obtain overlapping values of northward motion from both paleomagnetic and structural data will require: (i) identifying hidden faults or suture zones in the eastern Cordillera that may have contributed to overall higher Mesozoic northward motions than presently acknowledged; (ii) processing paleomagnetic data with new statistical standards, as this could lead to paleolatitude results that would require Mesozoic northward motions of lower amplitude than currently thought. This represents a clear opportunity for specialists of different disciplines to guide future joint research into understanding the source of discrepancies between their respective datasets. Such a community effort may be beneficial when paleomagnetic and structural data underpin research questions in other tectonic settings and in deeper time periods.

Acknowledgements

G.A. thanks the Swiss National Science Foundation for funding his stay at Utrecht University (grant #191102). We thank Erik van der Wiel and Nalan Lom for discussions and help in the paleomagnetic laboratory. We thank John Wakabayashi for discussions on Californian geology and the Franciscan complex. B.V., S.H.A.v.d.L., and D.J.J.v.H. were funded by NWO Vici grant 865.17.001. L.M.B. acknowledges NWO Veni grant 212.247.

Data availability statement

New paleomagnetic data can be imported into the Paleomagnetism.org 2.0 portal from data files (.col) available in the Supporting Information (Data Sets S1 and S2), as well as in the Paleomagnetism.org (link to be provided) and the MagIC (link to be provided) databases.

References

Alberts, D., Gehrels, G. E., & Nelson, J. (2021). U-Pb and Hf analyses of detrital zircons from Paleozoic and Cretaceous strata on Vancouver Island, British Columbia: Constraints on the Paleozoic tectonic evolution of southern Wrangellia. *Lithosphere, 2021*(1), 7866944. https://doi.org/10.2113/2021/7866944

Alvarez, W., Kent, D. V., Premoli Silva, I., Schweikert, R. A., & Larson, R.A. (1980). Franciscan Complex limestone deposited at 17° south paleolatitude. *Geological Society of America Bulletin, 91*, 476–484. https://doi.org/10.1130/0016-7606(1980)91<476:FCLDAS>2.0.CO;2

Amato, J. M., Pavlis, T.L., Clift, P. D., Kochelek, E. J., Hecker, J. P., Worthman, C. M., & Day, E. M. (2013). Architecture of the Chugach accretionary complex as revealed by detrital zircon ages and lithologic variations: Evidence for Mesozoic subduction erosion in south-central Alaska. *Geological Society of America Bulletin, 125*, 1891–1911. https://doi.org/10.1130/B30818.1

Amato, J. M., Rioux, M. E., Kelemen, P. B., Gehrels, G. E., Clift, P. D., Pavlis, T. L., & Draut, A. E. (2007). U-Pb geochronology of volcanic rocks from the Jurassic Talkeetna Formation and detrital zircons from prearc and postarc sequences: Implications for the age of magmatism and inheritance in the Talkeetna arc. *Geological Society of America Special Paper, 431*, 253–271. https://doi.org/10.1130/2007.2431(11)

Amaru, M. L. (2007). Global travel time tomography with 3-D reference models. *Geologica Ultraiectina, 274*, 174 p.

Andjić, G., Escuder-Viruete, J., Baumgartner-Mora, C., Baumgartner, P. O., Mitchell, S. F., Caron, M., & Caus, E. (2019). Sedimentary record of arc-continent collision along Mesozoic SW North America (Siuna Belt, Nicaragua). *Tectonics, 38* https://doi.org/10.1029/2019TC005741

Arkula, C., Lom, N., Wakabayashi, J., Rea-Downing, G., Qayyum, A., Dekkers, M. J., et al. (2023). The forearc ophiolites of California formed during trench-parallel spreading: Kinematic reconstruction of the western USA Cordillera since the Jurassic. *Earth-Science Reviews, 237*, 104275. https://doi.org/10.1016/j.earscirev.2022.104275

Bacon, C. R., Vazquez, J. A., & Wooden, J. L. (2012). Peninsular terrane basement ages recorded by Paleozoic and Paleoproterozoic zircon in gabbro xenoliths and andesite from Redoubt volcano, Alaska. *Geological Society of America Bulletin, 124*(1–2), 24–34. https://doi.org/10.1130/B30439.1

Bazard, D. R., Butler, R. F., Gehrels, G., & Soja, C. M. (1995). Early Devonian paleomagnetic data from the Lower Devonian Karheen Formation suggest Laurentia-Baltica connection for the Alexander terrane. *Geology, 23*(8), 707–710. https://doi.org/10.1130/0091-7613(1995)023<0707:EDPDFT>2.3.CO;2

Beck, M. E. (1976). Discordant paleomagnetic pole positions as evidence of regional shear in the western Cordillera of North America. *American Journal of Science, 276*, 694–712. https://doi.org/10.2475/ajs.276.6.694

Beck, M. E. (1980). Paleomagnetic record of plate-margin tectonic processes along the western edge of North America. *Journal of Geophysical Research, 85*(B12), 7115– 7131, https://doi.org/10.1029/JB085iB12p07115

Beck, M.E., & Noson, L. (1972). Anomalous paleolatitudes in Cretaceous granitic rocks: *Nature Physical Science, 235*, 11–13, https://doi.org/10.1038/physci235011a0

Beranek, L. P., van Staal, C. R., Gordee, S. M., McClelland, W. C., Israel, S., & Mihalynuk, M. G. (2012). Tectonic significance of Upper Cambrian–Middle Ordovician mafic volcanic rocks on the Alexander terrane, Saint Elias Mountains, northwestern Canada. *The Journal of Geology, 120*, 293–314. https://doi.org/10.1086/664788

Beranek, L. P., van Staal, C. R., McClelland, W. C., Joyce, N., & Israel, S. (2014). Late Paleozoic assembly of the Alexander-Wrangellia-Peninsular composite terrane, Canadian and Alaska Cordillera. *Geological Society of America Bulletin, 126*, 1531–1550. https://doi.org/10.1130/B31066.1

Boivin, M.-P., Matthews, W., Coutts, D., & Hubbard, S. (2022). Improved provenance constraints for Nanaimo Group sediments, British Columbia, Canada, through zircon LA-ICP-MS depth-profiling. *Tectonics, 41*, e2021TC007106. https://doi.org/10.1029/2021TC007106

Boschman, L. M., Garza, R. S. M., Langereis, C. G., & van Hinsbergen, D. J. J. (2018a). Paleomagnetic constraints on the kinematic relationship between the Guerrero terrane (Mexico) and North America since Early Cretaceous time. *Geological Society of America Bulletin, 130*(7–8), 1131–1142. https://doi.org/10.1130/B31916.1

Boschman, L. M., van der Wiel, E., Flores, K. E., Langereis, C. G., & van Hinsbergen, D. J. J. (2019). The Caribbean and Farallon plates connected: Constraints from stratigraphy and paleomagnetism of the Nicoya Peninsula, Costa Rica. *Journal of Geophysical Research Solid Earth, 124*, 6243–6266. https://doi.org/10.1029/2018JB016369

Boschman, L. M., & van Hinsbergen, D. J. J. (2016). On the enigmatic birth of the Pacific Plate within the Panthalassa Ocean. *Science Advances, 2*(7), e1600022, https://doi.org/10.1126/sciadv.1600022

Boschman, L. M., van Hinsbergen, D. J. J., Kimbrough, D. L., Langereis, C. G., & Spakman, W. (2018b). The dynamic history of 220 million years of subduction below Mexico: A correlation between slab geometry and overriding plate deformation based on geology, paleomagnetism, and seismic tomography. *Geochemistry, Geophysics, Geosystems, 19*(12), 4649–4672, https://doi.org/10.1029/2018GC007739

Boschman, L. M., van Hinsbergen, D. J. J., Langereis, C. G., Flores, K. E., Kamp, P. J. J., Kimbrough, D. L., et al. (2021a). Reconstructing lost plates and plate boundaries of the Panthalassa Ocean from circum-Pacific accretionary orogens. *American Journal of Science, 321*(6), 907–954, https://doi.org/10.2475/06.2021.08

Boschman, L. M., van Hinsbergen, D. J. J., & Spakman, W. (2021b). Reconstructing Jurassic-Cretaceous intra-oceanic subduction evolution in the northwestern Panthalassa Ocean using Ocean Plate Stratigraphy from Hokkaido, Japan. *Tectonics, 40*, e2019TC005673. https://doi.org/10.1029/2019TC005673

Busby, C.J., Morris, R.A., DeBari, S.M., Medynski, S., Putirka, K., Graham D.M.A., et al. (2023). Geology of a Large Intact Extensional Oceanic Arc Crustal Section with Superior Exposures: Cretaceous Alisitos Arc, Baja California (Mexico). *Geological Society of America Special Paper, 560*. https://doi.org/10.1130/2023.2560(01)

Butler, R. F., Gehrels, G. E., Baldwin, S., & Davidson, C. (2002). Paleomagnetism and geochronology of the Ecstall pluton in the Coast Mountains of British Columbia: Evidence for local deformation rather than large-scale transport. *Journal of Geophysical Research, 107*(B1), https://doi.org/10.1029/2001JB000270

Butler, R. F., Gehrels, G. E., Crawford, M. L., & Crawford, W. A. (2001a). Paleomagnetism of the Quottoon plutonic complex in the Coast Mountains of British Columbia and southeastern Alaska: evidence for tilting during uplift. *Canadian Journal of Earth Sciences, 38*(9), 1367–1384. https://doi.org/10.1139/e01-021

Butler, R. F., Gehrels, G. E., & Bazard, D. R. (1997). Paleomagnetism of Paleozoic strata of the Alexander terrane, southeastern Alaska. *Geological Society of America Bulletin, 109*(10), 1372–1388. https://doi.org/10.1130/0016-7606(1997)109<1372:POPSOT>2.3.CO;2

Butler, R. F., Gehrels, G. E., & Kodama, K. P. (2001b). A Moderate Translation Alternative to the Baja British Columbia Hypothesis. *GSA Today, 11*(6), 4–10.

Canil, D., Johnston, S.T., Larocque, J., Friedman, R., & Heaman, L.M. (2013). Age, construction, and exhumation of the midcrust of the Jurassic Bonanza arc, Vancouver Island, Canada. *Lithosphere*, *5* (1), 82–91. https://doi.org/10.1130/L225.1

Canil, D., Styan, J., Larocque, J., Bonnet, E., & Kyba, J. (2010). Thickness and composition of the Bonanza arc crustal section, Vancouver Island, Canada. *Geological Society of America Bulletin, 122*, 1094–1105. https://doi.org/10.1130/B26578.1

Caruthers, A. H., Marroquín, S. M., Gröcke, D. R., Golding, M. L., Aberhan, M., Them, T. R., et al. (2022). New evidence for a long Rhaetian from a Panthalassan succession (Wrangell Mountains, Alaska) and regional differences in carbon cycle perturbations at the Triassic-Jurassic transition. *Earth and Planetary Science Letters, 577*, 117262. https://doi.org/10.1016/j.epsl.2021.117262

Clennett, E. J., Sigloch, K., Mihalynuk, M.G., Seton, M., Henderson, M. A., Hosseini, K., et al. (2020). A quantitative tomotectonic plate reconstruction of western North America and the eastern Pacific basin. *Geochemistry, Geophysics, Geosystems, 20*, e2020GC009117. https://doi.org/10.1029/2020GC009117

Clift, P. D., Draut, A. E., Kelemen, P. B., Blusztajn, J., & Greene, A. (2005a). Stratigraphic and geochemical evolution of an oceanic arc upper crustal section: The Jurassic Talkeetna

Volcanic Formation, south-central Alaska. *Geological Society of America Bulletin, 117*, 902–925. https://doi.org/10.1130/B25638.1

Clift, P. D., Pavlis, T., DeBari, S. M., Draut, A. E., Rioux, M., & Kelemen, P. K. (2005b). Subduction erosion of the Jurassic Talkeetna-Bonanza arc and the Mesozoic accretionary tectonics of western North America. *Geology, 33*, 881–884. https://doi.org/10.1130/G21822.1

Colpron, M., & Nelson, J. L. (2009). A Palaeozoic Northwest Passage: incursion of Caledonian, Baltican and Siberian terranes into eastern Panthalassa, and the early evolution of the North American Cordillera. *The Geological Society, London, Special Publications, 318*, 273–307. https://doi.org/10.1144/SP318.10

Courtillot, V., Feiberg, H., Ragaru, J. P., Kerguelen, R., McWilliams, M., & Cox, A. (1985). Franciscan Complex limestone deposited at 24°N. *Geology, 13*, 107–110. https://doi.org/10.1130/0091-7613(1985)13<107:FCLDAN>2.0.CO;2

Cowan, D. S., Brandon, M., & Garver, J.I. (1997). Geologic tests of hypotheses for large coastwise displacements–a critique illustrated by the Baja British Columbia controversy. *American Journal of Science, 297*, 117–133. https://doi.org/10.2475/ajs.297.2.117

Dal Corso, J., Bernardi, M., Sun, Y., Song, H., Seyfullah, L. J., Preto, N., et al. (2020). Extinction and dawn of the modern world in the Carnian (Late Triassic). *Science Advances, 6*, eaba0099. https://doi.org/10.1126/sciadv.aba00

DeBari, S., Anderson, R. G., & Mortensen, J. K. (1999). Correlation among lower to upper crustal components in an island arc: The Jurassic Bonanza arc, Vancouver Island. Canada. *Canadian Journal of Earth Sciences, 36*, 1371–1413. https://doi.org/10.1139/e99-029

Deenen, M. H. L., Langereis, C. G., van Hinsbergen, D. J. J., & Biggin, A. J. (2011). Geomagnetic secular variation and the statistics of palaeomagnetic directions. *Geophysical Journal International, 186*(2), 509–520. https://doi.org/10.1111/j.1365-246X.2011.05050.x

Domeier, M., Doubrovine, P. V., Torsvik, T. H., Spakman, W., & Bull, A. L. (2016). Global correlation of lower mantle structure and past subduction. *Geophysical Research Letters, 43*(10), 4945–4953. https://doi.org/10.1002/2016GL068827

D'Souza, R. J., Canil, D., & Creaser, R. A. (2016). Assimilation, differentiation, and thickening during formation of arc crust in space and time: The Jurassic Bonanza arc, Vancouver Island, Canada. *Geological Society of America Bulletin, 128*(3–4), 543–557. https://doi.org/10.1130/B31289.1

Engebretson, D. C., Cox, A., & Gordon, R. G. (1985). Relative motions between oceanic and continental plates in the Pacific Basin. *Geological Society of America Special Paper, 206*, 59 p. https://doi.org/10.1130/SPE206-p1

Enkin, R. J., Baker, J., & Mustard, P. S. (2001). Paleomagnetism of the Upper Cretaceous Nanaimo Group, southwestern Canadian Cordillera. *Canadian Journal of Earth Sciences, 38*, 1403–1422. https://doi.org/10.1139/cjes-38-10-1403

Fisher, R. (1953). Dispersion on a sphere. *Proceedings of the Royal Society of London, Series A, Mathematical and Physical Sciences, 217*(1130), 295–305. https://doi.org/10.1098/rspa.1953.0064

Fuston, S., & Wu, J. (2019). Raising the Resurrection plate from an unfolded-slab plate tectonic reconstruction of northwestern North America since early Cenozoic time. *Geological Society of America Bulletin, 133* (5–6), 1128–1140. https://doi.org/10.1130/B35677.1

Gabrielse, H., Murphy, D. C., & Mortensen, J. K. (2006). Cretaceous and Cenozoic dextral orogen-parallel displacements, magmatism, and paleogeography, north-central Canadian Cordillera. *Geological Association of Canada Special Paper, 46*, 255–276.

Gehrels, G., Rusmore, M., Woodsworth, G., Crawford, M., Andronicos, C., Hollister, L., et al. (2009). U–Th–Pb geochronology of the Coast Mountains batholith in north-coastal British Columbia: constraints on age and tectonic evolution. *Geological Society of America Bulletin, 121*(9–10), 1341–1361. https://doi.org/10.1130/B26404.1

Gehrels, G. E., & Saleeby, J. B. (1987). Geologic framework, tectonic evolution, and displacement history of the Alexander terrane. *Tectonics, 6*, 151–173. https://doi.org/10.1029/TC006i002p00151

Gerritsen, D., Vaes, B., & van Hinsbergen, D. J. J. (2022). Influence of data filters on the position and precision of paleomagnetic poles: What is the optimal sampling strategy? *Geochemistry, Geophysics, Geosystems, 23*, e2021GC010269. https://doi.org/10.1029/2021GC010269

Greene, A. R., Scoates, J. S., Weis, D., Katvala, E. C., Israel, S., & Nixon, G.T. (2010). The architecture of oceanic plateaus revealed by the volcanic stratigraphy of the accreted Wrangellia oceanic plateau. *Geosphere, 6*(1), 47–73. https://doi.org/10.1130/GES00212.1

Grommé, S., & Hillhouse, J.W. (1997). Paleomagnetic results from Devonian and Permian rocks at Saginaw Bay, Kuiu Island, southeastern Alaska. *United States Geological Survey Professional Paper, 1574*, 295–306.

Guilmette, C., Smit, M., van Hinsbergen, D. J. J., Gürer, D., Maffione, M., Rabeau, O., & Savard, D. (2018). Forced subduction initiation recorded in the sole and crust of the Semail ophiolite of Oman. *Nature Geoscience, 11*, 688–695. https://doi.org/10.1038/s41561-018-0209-2

Haeussler, P. J., Coe, R. S., & Onstott, T. C. (1992a). Paleomagnetism of the Late Triassic Hound Island Volcanics: revisited. *Journal of Geophysical Research, 97*, 19617–19639. https://doi.org/10.1029/92JB01361

Haeussler, P. J., Coe, R. S., & Renne, P. (1992b). Paleomagnetism and geochronology of 23 Ma gabbroic intrusions in the Keku Strait, Alaska, and implications for the Alexander terrane. *Journal of Geophysical Research, 97*(B13), 19641–19651. https://doi.org/10.1029/92JB01360

Hampton, B. A., Ridgway, K. D., & Gehrels, G. E. (2010). A detrital record of Mesozoic island arc accretion and exhumation in the North American Cordillera: U-Pb geochronology of the

Kahiltna basin, southern Alaska. *Tectonics, 29*, TC4015. https://doi.org/10.1029/2009tc002544

Harbert, W. (1990). Paleomagnetic data from Alaska: Reliability, interpretation and terrane trajectories. *Tectonophysics, 184*, 111–135. https://doi.org/10.1016/0040-1951(90)90124-Q

Hillhouse, J. W. (1977). Paleomagnetism of the Triassic Nikolai Greenstone, south-central Alaska. *Canadian Journal of Earth Sciences, 14*, 2578–2592. https://doi.org/10.1139/e77-223

Hillhouse, J. W. (1987). Accretion of southern Alaska. *Tectonophysics, 139*, 107–122. https://doi.org/10.1016/0040-1951(87)90200-9

Hillhouse, J. W., & Grommé, C. S. (1984). Northward displacement and accretion of Wrangellia: New paleomagnetic evidence from Alaska. *Journal of Geophysical Research, 89*, 4461–4477. https://doi.org/10.1029/JB089iB06p04461

Hillhouse, J. W., Grommé, C. S., & Csejtey, B. (1985). Tectonic implications of paleomagnetic poles from Lower Tertiary Volcanic Rocks, south central Alaska. *Journal of Geophysical Research, 90*(B14), 12523– 12535. https://doi.org/10.1029/JB090iB14p12523

Hollister, L. S., Hargraves, R. B., James, T. S., & Renne, P. R. (2004). The paleomagnetic effects of reheating the Ecstall pluton, British Columbia. E*arth and Planetary Science Letters, 221*(1–4), 397–407. https://doi.org/10.1016/S0012-821X(04)00067-6

Housen, B. A., & Beck, M. E. (1999). Testing terrane transport: An inclusive approach to the Baja B.C. controversy. *Geology, 27(*12), 1143–1146. https://doi.org/10.1130/0091-7613(1999)027<1143:tttaia>2.3.co;2

Hults, C. P., Wilson, F. H., Donelick, R. A., & O'Sullivan, P. B. (2013). Two flysch belts having distinctly different provenance suggest no stratigraphic link between the Wrangellia composite terrane and the paleo-Alaskan margin. *Lithosphere, 5*(6), 575–594. https://doi.org/10.1130/L310.1

Irving, E. (1985). Whence British Columbia? *Nature, 314*, 673–674. https://doi.org/10.1038/314673a0

Irving, E., & Brandon, M. T. (1990). Paleomagnetism of the Flores volcanics, Vancouver Island, in place by Eocene time. *Canadian Journal of Earth Sciences, 27*, 811–817. https://doi.org/10.1139/e90-083

Irving, E., & Massey, N. W. D. (1990). Paleomagnetism of ocean layers 2 and 3: evidence from the Metchosin Complex, Vancouver Island. *Physics of the Earth and Planetary Interiors, 64*(2–4), 247–260. https://doi.org/10.1016/0031-9201(90)90041-U

Irving, E., Woodsworth, G. J., Wynne, P. J., & Morrison, A. (1985). Paleomagnetic evidence for displacement from the south of the Coast Plutonic Complex, British Columbia. *Canadian Journal of Earth Sciences, 22*, 584–598. https://doi.org/10.1139/e85-058

Irving, E., & Yole, R. W. (1987). Tectonic rotations and translations in Western Canada—New evidence from Jurassic rocks of Vancouver Island. *Geophysical Journal of the Royal Astronomical Society, 91*, 1025–1048. https://doi.org/10.1111/j.1365-246X.1987.tb01678.x

Isozaki, Y., Maruyama, S., & Furuoka, F. (1990). Accreted oceanic materials in Japan. *Tectonophysics, 181*, 179–205. https://doi.org/10.1016/0040-1951(90)90016-2

Israel, S., Beranek, L. P., Friedman, R. M., & Crowley, J. L. (2014). New ties between the Alexander terrane and Wrangellia and implications for North America Cordilleran evolution. *Lithosphere, 6*, 270–276. https://doi.org/10.1130/L364.1

Jarboe, N. A., Koppers, A. A., Tauxe, L., Minnett, R., & Constable, C. (2012). The online MagIC Database: data archiving, compilation, and visualization for the geomagnetic, paleomagnetic and rock magnetic communities. *American Geophysical Union, Fall Meeting 2012*, GP31A–1063.

Johnson, C. L., Constable, C. G., Tauxe, L., Barendregt, R., Brown, L. L., Coe, R. S., et al. (2008). Recent investigations of the 0-5 Ma geomagnetic field recorded by lava flows.

Geochemistry, Geophysics, Geosystems, *9*(4), Q04032. https://doi.org/10.1029/2007GC001696

Johnston, S. T. (2001). The Great Alaskan Terrane Wreck: Reconciliation of paleomagnetic and geological data in the Northern Cordillera. *Earth and Planetary Science Letters, 193*, 259–272. https://doi.org/10.1016/S0012-821X(01)00516-7

Johnston, S. T. (2008). The Cordilleran ribbon continent of North America. *Annual Review of Earth and Planetary Sciences, 36*, 495–530. https://doi.org/10.1146/annurev.earth.36.031207.124331

Kent, D. V., & Irving, E. (2010). Influence of inclination error in sedimentary rocks on the Triassic and Jurassic apparent pole wander path for North America and implications for Cordilleran tectonics. *Journal of Geophysical Research, 115*, B10103. https://doi.org/10.1029/2009JB007205

Kim, B., & Kodama, K. P. (2004). A compaction correction for the paleomagnetism of the Nanaimo Group sedimentary rocks: implications for the Baja British Columbia hypothesis. *Journal of Geophysical Research, 109*, B02102. https://doi.org/10.1029/2003JB002696

Kirschvink, J. L. (1980). The least-squares line and plane and the analysis of palaeomagnetic data. *Geophysical Journal International, 62*(3), 699–718. https://doi.org/10.1111/j.1365-246X.1980.tb02601.x

Koymans, M. R., Langereis, C. G., Pastor-Galan, D., & van Hinsbergen, D. J. J. (2016). Paleomagnetism.org: an online multi-platform open source environment for paleomagnetic data analysis. *Computers & Geosciences, 93*, 127–137. https://doi.org/10.1016/j.cageo.2016.05.007

Koymans, M. R., van Hinsbergen, D. J. J., Pastor-Galan, D., Vaes, B., & Langereis, C. G. (2020). Towards FAIR paleomagnetic data management through Paleomagnetism. org 2.0. *Geochemistry, Geophysics, Geosystems, 21*(2), e2019GC008838. https://doi.org/10.1029/2019GC008838

Krijgsman, W., & Tauxe, L. (2006). E/I corrected paleolatitudes for the sedimentary rocks of the Baja British Columbia hypothesis. *Earth and Planetary Science Letters, 242*, 205–216. https://doi.org/10.1016/j.epsl.2005.11.052

Kuniyoshi, S., & Liou J. G. (1976). Burial metamorphism of the Karmutsen volcanic rocks, northeastern Vancouver Island, British Columbia. *American Journal of Science, 276* (9), 1096–1119. https://doi.org/10.2475/ajs.276.9.1096

Lei, J. Z. X., Golding, M. L., & Husson, J. M. (2020). Analyzing spatial patterns of thermal alteration in the Stikine and Wrangell terranes of the Canadian Cordillera using the conodont color alteration index (CAI) to identify hot spots and cold spots. *Geological Survey of Canada Open File, 8746*, 43 p. https://doi.org/10.4095/327243

Mahoney, J. B., Haggart, J. W., Grove, M., Kimbrough, D. L., Isava, V., Link, P. K., et al. (2021). Evolution of the Late Cretaceous Nanaimo Basin, British Columbia, Canada: Definitive provenance links to northern latitudes. *Geosphere, 17*(6), 2197–2233. https://doi.org/10.1130/GES02394.1

Mahoney, J. B., Mustard, P. S., Haggart, J. W., Friedman, R. M., Fanning, C. M., Mcnicoll, V. J., & Charlotte, Q. (1999). Archean zircons in Cretaceous strata of the western Canadian Cordillera: The "Baja B.C." hypothesis fails a "crucial test". *Geology, 27*(3), 195–198. https://doi.org/10.1130/0091-7613(1999)027<0195:azicso>2.3.co;2

Manselle, P., Brueseke, M. E., Trop, J. M., Benowitz, J. A., Snyder, D. C., & Hart, W. K. (2020). Geochemical and stratigraphic analysis of the Chisana Formation, Wrangellia terrane, eastern Alaska: Insights into Early Cretaceous magmatism and tectonics along the northern Cordilleran margin. *Tectonics, 39*, e2020TC006131. https://doi.org/10.1029/2020TC006131

Martini, M., Solari, L., & López-Martínez, M. (2014). Correlating the Arperos Basin from Guanajuato, central Mexico, to Santo Tomás, southern Mexico: Implications for the paleogeography and origin of the Guerrero terrane. *Geosphere, 10*(6), 1385–1401. https://doi.org/10.1130/GES01055.1

Matthews, W. A., Guest, B., Coutts, D. S., Bain, H., & Hubbard, S. M. (2017). Detrital zircons from the Nanaimo Basin, Vancouver Island, British Columbia: An independent test of Late Cretaceous to Cenozoic northward translation. *Tectonics, 36*(5), 854–876. https://doi.org/10.1002/2017TC004531

McClelland, W. C., Gehrels, G. E., & Saleeby, J. B. (1992). Upper Jurassic–Lower Cretaceous basinal strata along the Cordilleran margin: Implications for the accretionary history of the Alexander-Wrangellia-Peninsular terrane. *Tectonics, 11*, 823–835. https://doi.org/10.1029/92TC00241

McLaughlin, R. J., Kling, S. A., Poore, R. Z., McDougall, K., & Beutner, E. C. (1982). Post-middle Miocene Accretion of Franciscan Rocks, Northwestern California. *Geological Society of America Bulletin, 93*, 595–605. https://doi.org/10.1130/0016-7606(1982)93<595:pmaofr>2.0.co;2

McFadden, P., & McElhinny, M. (1988). The combined analysis of remagnetization circles and direct observations in palaeomagnetism. *Earth and Planetary Science Letters, 87*(1–2), 161–172. https://doi.org/10.1016/0012-821X(88)90072-6

Meert, J. G., Pivarunas, A. F., Evans, D. A. D., Pisarevsky, S. A., Pesonen, L. J., Li, Z.-X., et al. (2020). The magnificent seven: A proposal for modest revision of the Van der Voo (1990) quality index. *Tectonophysics, 790*, 228549. https://doi.org/10.1016/j.tecto.2020.228549

Monger, J. W. H. (2014). Logan Medallist 1. Seeking the suture: The Coast-Cascade conundrum. *Geoscience Canada, 41*, 1–20. https://doi.org/10.12789/geocanj.2014.41.058

Monger, J. W. H., & Price, R. A. (1996). Comment on "Paleomagnetism of the Upper Cretaceous strata of Mount Tatlow: Evidence for 3000 km of northward displacement of the eastern Coast Belt, British Columbia" by P. J. Wynne et al., and on "Paleomagnetism of the Spences Bridge Group and northward displacement of the Intermontane Belt, British Columbia: A second look" by E. Irving et al. *Journal of Geophysical Research, 101*(B6), 13793–13799. https://doi.org/10.1029/96JB00795

Morris, R., & Canil, D. (2022). CO2 transport at shallow depths in arc magmas: evidence from unique orbicular dikes in the Jurassic Bonanza arc, Vancouver Island, Canada. *Contributions to Mineralogy and Petrology, 177* (6). https://doi.org/10.1007/s00410-021-01852-y

Mulcahy, S. R., Starnes, J. K., Day, H. W., Coble, M. A., & Vervoort, J. D. (2018). Early onset of Franciscan subduction. *Tectonics, 37*, 1194–1209. https://doi.org/10.1029/2017TC004753

Mullender, T. A. T., van Velzen, A. J., & Dekkers, M. J. (1993). Continuous drift correction and separate identification of ferromagnetic and paramagnetic contributions in thermomagnetic runs. *Geophysical Journal International, 114*, 663–672. https://doi.org/10.1111/j.1365-246X.1993.tb06995.x

Mullender, T. A., Frederichs, T., Hilgenfeldt, C., de Groot, L. V., Fabian, K., & Dekkers, M. J. (2016). Automated paleomagnetic and rock magnetic data acquisition with an in-line horizontal "2G" system. *Geochemistry, Geophysics, Geosystems, 17*, 3546–3559. https://doi.org/10.1002/2016GC006436

Nelson, J., & Colpron, M. (2007). Tectonics and metallogeny of the British Columbia, Yukon and Alaskan Cordillera, 1.8 Ga to the present. *Geological Association of Canada Mineral Deposits Division Special Publication, 5*, 755–791.

Nixon, G. T., Hammack, J. L., Hamilton, J. V., Jennings, H., Larocque, J. P., Orr, A. J., et al. (2011a). Geology, Geochronology, Lithogeochemistry and Metamorphism of the Mahatta Creek Area, Northern Vancouver Island. *British Columbia Geological Survey Geoscience Map, 2011-3*, 1:50 000 scale.

Nixon, G. T., Hammack, J. L., Koyanagi, V. M., Payie, G. J., Orr, A. J., Haggart, J. W., et al. (2011b). Geology, Geochronology, Lithogeochemistry and Metamorphism of the Quatsino-Port McNeill Area, Northern Vancouver Island. *British Columbia Geological Survey Geoscience Map, 2011-2*, 1:50 000 scale.

Nixon, G. T., Hammack, J.L., Koyanagi, V. M., Snyder, L. D., Payie, G. J., Panteleyev, A., et al. (2011c). Geology, Geochronology, Lithogeochemistry and Metamorphism of the Holberg-Winter Harbour Area, Northern Vancouver Island. *British Columbia Geological Survey Geoscience Map, 2011-1*, 1:50 000 scale.

Nixon, G. T., & Orr, A. J. (2007). Recent revisions to the Early Mesozoic stratigraphy of northern Vancouver Island (NTS 102I; 92L) and metallogenic implications, British Columbia. *British Columbia Ministry of Energy, Mines and Petroleum Resources, Geological Fieldwork 2006, Paper 2007-1*, 163–177.

Nixon, G.T., Snyder, L.D., Payie, G.J., Long, S., Finnie, A., Orr, A.J., et al. (2011d). Geology, Geochronology, Lithogeochemistry and Metamorphism of the Alice Lake Area, Northern Vancouver Island. *British Columbia Geological Survey Geoscience Map, 2011-4*, 1:50 000 scale.

Nokleberg, W. J., Bundtzen, T. K., Eremin, R. A., Ratkin, V. V., Dawson, K. M., Shpikerman, V.I., et al. (2005). In: Metallogenesis and Tectonics of the Russian Far East, Alaska and the Canadian Cordillera. *United States Geological Survey Professional Paper, 1697*, 397 p.

Nokleberg, W. J., Parfenov, L. M., Monger, J. W. H., Baranov, B. V., Byalobzhesky, S. G., Bundtzen, T.K., et al. (1994). Circum-North Pacific tectono-stratigraphic terrane map. *United States Geological Survey Open-File Report, 94–714*, 210 p., 4 sheets, scales 1:5,000,000, 1:10,000,000.

Nokleberg, W. J., Parfenov, L. M., Monger, J. W. H., Norton, I. O., Khanchuk, A. I., Stone, D. B., et al. (2000). Phanerozoic tectonic evolution of the Circum-North Pacific. *United States Geological Survey Professional Paper, 1626*, 122 p.

Opdyke, N. D., & Channell, J. E. T. (1996). Magnetic Stratigraphy. San Diego, CA: Academic Press, 346 p.

Panuska, B. C., Decker, J. E., & Berg, H. C. (1984). A preliminary paleomagnetic study of the Gravina-Nutzotin belt, southern and southeastern Alaska. *United States Geological Survey Circular, 868*, 117–120.

Panuska, B. C., & Stone, D. B. (1981). Late Paleozoic paleomagnetic data for Wrangellia; resolution of the polarity ambiguity. *Nature, 293*, 561–563. https://doi.org/10.1038/293561a0

Panuska, B. C. (1985). Paleomagnetic evidence for a post-Cretaceous accretion of Wrangellia. *Geology, 13*, 880–883. https://doi.org/10.1130/0091-7613(1985)13<880:PEFAPA>2.0.CO;2

Parsons, A. J., Sigloch, K., & Hosseini, K. (2021). Australian plate subduction is responsible for northward motion of the India-Asia collision zone and ∼1,000 km lateral migration of the Indian slab. *Geophysical Research Letters, 48*, e2021GL094904. https://doi.org/10.1029/2021GL094904

Passier, H. F., de Lange, G. J., & Dekkers, M. J. (2001). Rock-magnetic properties and geochemistry of the active oxidation front and the youngest sapropel in the Mediterranean. *Geophysical Journal International, 145*, 604–614. https://doi.org/10.1046/j.0956-540x.2001.01394.x

Pavlis, T. L., Amato, J. M., Trop, J. M., Ridgway, K. D., Roeske, S. M., & Gehrels, G. E. (2019). Subduction polarity in ancient arcs: a call to integrate geology and geophysics to decipher the Mesozoic tectonic history of the northern Cordillera of North America. *GSA Today, 29*, 4–10. https://doi.org/10.1130/GSATG402A.1

Pavlis, T. L., Amato, J. M., Trop, J. M., Ridgway, K. D., Roeske, S. M. & Gehrels, G. E. (2020). Subduction polarity in ancient arcs: A call to integrate geology and geophysics to decipher the Mesozoic tectonic history of the Northern Cordillera of North America: Reply. *GSA Today, 30*, 51–58. https://doi.org/10.1130/GSATG465Y.1

Plafker, G., & Berg, H. D. (1994). Overview of the geology and tectonic evolution of Alaska. In: Plafker, G., Berg, H. C. (Eds.), The geology of Alaska. *GSA Decade of North American Geology, G–1*, 989–1021. https://doi.org/10.1130/DNAG-GNA-G1.989

Plafker, G., Nokleberg, W. J., & Lull, J. S. (1989). Bedrock geology and tectonic evolution of the Wrangellia, Peninsular, and Chugach terranes along the Trans-Alaskan crustal transect in the northern Chugach Mountains and southern Copper River basin, Alaska. *Journal of Geophysical Research, 94*, 4255–4295. https://doi.org/10.1029/JB094iB04p04255

Qayyum, A., Lom, N., Advokaat, E. L., Spakman, W., van der Meer, D. G., & van Hinsbergen, D. J. J. (2022). Subduction and slab detachment under moving trenches during ongoing India-Asia convergence. *Geochemistry, Geophysics, Geosystems, 23*, e2022GC010336. https://doi.org/10.1029/2022GC010336

Rioux, M., Hacker, B., Mattinson, J., Kelemen, P., Blusztajn, J., & Gehrels, G. (2007). Magmatic development of an intra-oceanic arc: High-precision U-Pb zircon and whole-rock isotopic analyses from the accreted Talkeetna arc, south-central Alaska. *Geological Society of America Bulletin, 119*, 1168–1184. https://doi.org/10.1130/B25964.1

Rioux, M., Mattinson, J., Hacker, B., Kelemen, P., Blusztajn, J., Hanghøj, K., & Gehrels, G. (2010). Intermediate to felsic middle crust in the accreted Talkeetna arc, the Alaska Peninsula and Kodiak Island, Alaska: An analogue for low-velocity middle crust in modern arcs. *Tectonics, 29*, TC3001. https://doi.org/10.1029/2009TC002541

Roeske, S. M., Mattinson, J. M., & Armstrong, R. L. (1989). Isotopic ages of glaucophane schists on the Kodiak Islands, southern Alaska, and their implications for the Mesozoic tectonic history of the Border Ranges fault system. *Geological Society of America Bulletin, 101*, 1021–1037. https://doi.org/10.1130/0016-7606(1989)101<1021:IAOGSO>2.3.CO;2

Rowley, D. B. (2019). Comparing paleomagnetic study means with apparent wander paths: A case study and paleomagnetic test of the Greater India versus Greater Indian Basin hypotheses. *Tectonics, 38*, 722–740. https://doi.org/10.1029/2017TC004802

Rusmore, M. E., Bogue, S. W., & Woodsworth, G. J. (2013). Paleogeography of the Insular and Intermontane terranes reconsidered: Evidence from the southern Coast Mountains Batholith, British Columbia. *Lithosphere, 5*, 521–536. https://doi.org/10.1130/10.1130/L288.1

Saleeby, J. B. (2000). Geochronologic investigations along the Alexander-Taku terrane boundary, southern Revillagigedo Island to Cape Fox areas, southeast Alaska. *Geological Society of America Special Paper, 343*, 107–143. https://doi.org/10.1130/0-8137-2343-4.107

Sauer, K. B., Gordon, S. M., Miller, R. B., Jacobson, C. E., Grove, M., Vervoort, J. D., & Fisher, C. M. (2019). Deep-crustal metasedimentary rocks support Late Cretaceous "Mojave BC" translation. *Geology, 47*(2), 1–4. https://doi.org/10.1130/G45554.1

Scotese, C. R. (2021). An atlas of Phanerozoic paleogeographic maps: the seas come in and the seas go out. *Annual Review of Earth and Planetary Sciences, 49*, 679–728. https://doi.org/10.1146/annurev-earth-081320-064052

Seton, M., Müller, R. D., Zahirovic, S., Gaina, C., Torsvik, T., Shephard, G., et al. (2012). Global continental and ocean basin reconstructions since 200 Ma. *Earth-Science Reviews, 113*(3–4), 212–270. https://doi.org/10.1016/j.earscirev.2012.03.002

Sigloch, K., McQuarrie, N., & Nolet, G. (2008). Two-stage subduction history under North America inferred from multiple-frequency tomography. *Nature Geoscience, 1*, 458–462. https://doi.org/10.1038/ngeo231

Sigloch, K., & Mihalynuk, M. G. (2013). Intra-oceanic subduction shaped the assembly of Cordilleran North America. *Nature, 496*, 50–56. https://doi.org/10.1038/nature12019

Sigloch, K., & Mihalynuk, M. G. (2020). Comment on GSA Today article by Pavlis et al., 2019: "Subduction Polarity in Ancient Arcs: A Call to Integrate Geology and Geophysics to Decipher the Mesozoic Tectonic History of the Northern Cordillera of North America". *GSA Today, 30*, 47–50. https://doi.org/10.1130/GSATG431C.1

Sigloch, K., & Mihalynuk, M. G. (2017). Mantle and geological evidence for a Late Jurassic–Cretaceous suture spanning North America. *Geological Society of America Bulletin, 129*(11–12), 1489–1520. https://doi.org/10.1130/B31529.1

Sisson, V., & Onstott, T. (1986). Dating blueschist metamorphism–A combined Ar-40/Ar-39 and electron microprobe approach. *Geochimica et Cosmochimica Acta, 50*, 2111–2117. https://doi.org/10.1016/0016-7037(86)90264-4

Snortum, E., & Day, J. M. D. (2020). Forearc origin for Coast Range Ophiolites inferred from osmium isotopes and highly siderophile elements. *Chemical Geology, 550*, 119723. https://doi.org/10.1016/j.chemgeo.2020.119723

Spakman, W., Chertova, M. V., Van Den Berg, A., & van Hinsbergen, D. J. J. (2018). Puzzling features of western Mediterranean tectonics explained by slab dragging. *Nature Geoscience, 11*(3), 211–216. https://doi.org/10.1038/s41561-018-0066-z

Stamatakos, J. A., Trop, J. M., & Ridgway, K. D. (2001). Late Cretaceous paleogeography of Wrangellia: paleomagnetism of the MacColl Ridge Formation, southern Alaska, revisited. *Geology, 29*(10), 947–950. https://doi.org/10.1130/0091-7613(2001)029<0947:LCPOWP>2.0.CO;2

Steinberger, B., & Torsvik, T. (2008). Absolute plate motions and true polar wander in the absence of hotspot tracks. *Nature, 452*, 620–623. https://doi.org/10.1038/nature06824

Stevens Goddard, A. L., Trop, J. M., & Ridgway, K. D. (2018). Detrital zircon record of a Mesozoic collisional forearc basin in south central Alaska: The tectonic transition from an oceanic to continental arc. *Tectonics, 37*, 529–557. https://doi.org/10.1002/2017TC004825

Stewart, R.J., & Page, R.J. (1973). Zeolite facies metamorphism of the Late Cretaceous Nanaimo Group, Vancouver Island and Gulf Islands, British Columbia. *Canadian Journal of Earth Sciences, 11*, 280–284. https://doi.org/10.1139/e74-024

Stone, D. B., Panuska, B. C., & Packer, D. R. (1982). Paleolatitudes versus time for southern Alaska. *Journal of Geophysical Research, 87*(B5), 3697–3707. https://doi.org/10.1029/JB087iB05p03697

Symons, D. T. A. (1973). Paleomagnetic zones in the Oligocene East Sooke Gabbro, Vancouver Island, British Columbia. *Journal of Geophysical Research, 78*(23), 5100–5109. https://doi.org/10.1029/JB078i023p05100

Symons, D. T. A. (1985). Paleomagnetism of the westcoast complex and the geotectonics of the Vancouver island segment of the wrangellian subterrane. *Journal of Geodynamics, 2* (2–3), 211–228. https://doi.org/10.1016/0264-3707(85)90011-0

Tarduno, J. A., McWilliams, M., Debiche, M. G., Sliter, W. V., & Blake, Jr., M.C. (1985). Franciscan Complex Calera limestones: accreted remnants of Farallon plate oceanic plateaus. *Nature, 317*, 345–347. https://doi.org/10.1038/317345a0

Tarduno, J. A., McWilliams, M., Sliter, W. V., Cook, H. E., Blake, Jr., M. C., & Premoli Silva, I. (1986). Southern hemisphere origin of the Cretaceous Laytonville Limestone of California. *Science, 231*, 1425–1428. https://doi.org/10.1126/science.231.4744.142

Tauxe, L. (2010). Essentials of paleomagnetism. 512 p. Berkeley, University of California Press.

Tauxe, L. & Kent, D. V. (2004). A Simplified Statistical Model for the Geomagnetic Field and the Detection of Shallow Bias in Paleomagnetic Inclinations: was the Ancient Magnetic Field Dipolar? *Geophysical Monograph Series, 145*, 101–116. https://doi.org/10.1029/145GM08

Tauxe, L., Kodama, K., & Kent, D. V. (2008). Testing corrections for paleomagnetic inclination error in sedimentary rocks: a comparative approach. *Physics of the Earth and Planetary Interiors, 169*, 152–165. https://doi.org/10.1016/j.pepi.2008.05.006

Tauxe, L., & Watson, G. S. (1994). The fold test–An Eigen analysis approach. *Earth and Planetary Science Letters, 122*(3–4), 331–341. https://doi.org/10.1016/0012-821X(94)90006-X

Tikoff, B., Housen, B. A., Maxson, J. A., Nelson, E. M., Trevino, S., & Shipley, T. F. (2023). Hit-and-run model for Cretaceous–Paleogene tectonism along the western margin of Laurentia.

Memoirs - Geological Society of America, 220, 659–705. https://doi.org/10.1130/2022.1220(32)

Torsvik, T. H., van der Voo, R., Preeden, U., MacNiocaill, C., Steinberger, B., Doubrovine, et al. (2012). Phanerozoic polar wander, palaeogeography and dynamics. *Earth-Science Reviews, 114*, 325–368. https://doi.org/10.1016/j.earscirev.2012.06.007

Trop, J.M., & Ridgway, K.D. (2007). Mesozoic and Cenozoic tectonic growth of southern Alaska: A sedimentary basin perspective. *Geological Society of America Special Paper, 431*, pp. 55–94. https://doi.org/10.1130/2007.2431(04)

Trop, J. M., Ridgway, K. D., Manuszak, J. D., & Layer, P. (2002). Mesozoic sedimentary-basin development on the allochthonous Wrangellia composite terrane, Wrangell Mountains basin Alaska: a long-term record of terrane migration and arc construction. *Geological Society of America Bulletin, 114*, 693–717. https://doi.org/10.1130/0016-7606(2002)114<0693:MSBDOT>2.0.CO;2

Umhoefer, P. J. (1987). Northward translation of Baja British Columbia along the Late Cretaceous to Paleocene margin of western North America. *Tectonics, 6*, 377–394. https://doi.org/10.1029/TC006i004p00377

Van der Voo, R., Jones, M., Grommé, C. S., Eberlein, G. D., & Churkin, M. (1980). Paleozoic paleomagnetism and northward drift of the Alexander Terrane, southeastern Alaska. *Journal of Geophysical Research, 85*(B10), 5281– 5296. https://doi.org/10.1029/JB085iB10p05281

Vaes, B. (2023). On pole position: new approaches to quantifying polar wander and relative paleomagnetic displacements. *Utrecht Studies in Earth Sciences, 283*, 269 p. https://doi.org/10.33540/1794

Vaes, B., Gallo, L. C., & van Hinsbergen, D. J. J. (2022). On pole position: causes of dispersion of the paleomagnetic poles behind apparent polar wander paths. *Journal of Geophysical Research Solid Earth, 127*(4), e2022JB023953. https://doi.org/10.1029/2022JB023953

Vaes, B., Li, S., Langereis, C. G., & van Hinsbergen, D. J. J. (2021). Reliability of palaeomagnetic poles from sedimentary rocks. *Geophysical Journal International, 225*(2), 1281–1303. https://doi.org/10.1093/gji/ggab016

Vaes, B., van Hinsbergen, D.J.J., van de Lagemaat, S.H.A., van der Wiel, E., Lom, N., Advokaat, E.L., et al. (2023). A global apparent polar wander path for the last 320 Ma calculated from site-level paleomagnetic data. *Earth-Science Reviews,* 104547. https://doi.org/10.1016/j.earscirev.2023.104547

van de Lagemaat, S. H., Kamp, P. J., Boschman, L. M., & van Hinsbergen, D. J. J. (2023). Reconciling the Cretaceous breakup and demise of the Phoenix Plate with East Gondwana orogenesis in New Zealand. *Earth-Science Reviews, 236*, 104276. https://doi.org/10.1016/j.earscirev.2022.104276

van de Lagemaat, S. H. A., van Hinsbergen, D. J. J., Boschman, L. M., Kamp, P. J. J., & Spakman, W. (2018). Southwest Pacific absolute plate kinematic reconstruction reveals major Cenozoic Tonga-Kermadec slab dragging. *Tectonics, 37*, 2647–2674. https://doi.org/10.1029/2017TC004901

van der Meer, D. G., Spakman, W., van Hinsbergen, D. J. J., Amaru, M. L., & Torsvik, T. H. (2010). Towards absolute plate motions constrained by lower-mantle slab remnants. *Nature Geoscience, 3*(1), 36–40. https://doi.org/10.1038/ngeo708

van der Meer, D. G., Torsvik, T. H., Spakman, W., van Hinsbergen, D. J. J., & Amaru, M. L. (2012). Intra-Panthalassa Ocean subduction zones revealed by fossil arcs and mantle structure. *Nature Geoscience, 5*(3), 215–219. https://doi.org/10.1038/ngeo1401

van der Meer, D. G., van Hinsbergen, D. J. J., & Spakman, W. (2018). Atlas of the Underworld: Slab remnants in the mantle, their sinking history, and a new outlook on lower mantle viscosity. *Tectonophysics, 723*, 309–448. https://doi.org/10.1016/j.tecto.2017.10.004

van Velzen, A. J., & Zijderveld, J. (1995). Effects of weathering on single-domain magnetite in Early Pliocene marine marls. *Geophysical Journal International, 121*(1), 267–278. https://doi.org/10.1111/j.1365-246X.1995.tb03526.x

Wakabayashi, J. (2015). Anatomy of a subduction complex: architecture of the franciscan complex, California, at multiple length and time scales. *International Geology Review, 57*, 669–746. https://doi.org/10.1080/00206814.2014.998728

Ward, P. D., Hurtado, J. M., Kirschvink, J. L., & Verosub, K. L. (1997). Measurements of the Cretaceous Paleolatitude of Vancouver Island: consistent with the Baja–British Columbia Hypothesis. *Science, 277*, 1642–1645. https://doi.org/10.1126/science.277.5332.16

White, C., Gehrels, G. E., Pecha, M., Giesler, D., Yokelson, I., McClelland, W. C., & Butler, R. F. (2016). U-Pb and Hf isotope analysis of detrital zircons from Paleozoic strata of the southern Alexander terrane (Southeast Alaska). *Lithosphere, 8*(1), 83–96. https://doi.org/10.1130/L475.1

Wright, N. M., Seton, M., Williams, S. E., & Müller, R. D. (2016). The Late Cretaceous to recent tectonic history of the Pacific Ocean basin. *Earth-Science Reviews, 154*, 138–173. https://doi.org/10.1016/j.earscirev.2015.11.015

Yokelson, I., Gehrels, G. E., Pecha, M., Giesler, D., White, C., & McClelland, W. C. (2015). U-Pb and Hf isotope analysis of detrital zircons from Mesozoic strata of the Gravina belt, southeast Alaska. *Tectonics, 34*, 2052–2066. https://doi.org/10.1002/2015TC003955

Yole, R. W., & Irving, E. (1980). Displacement of Vancouver Island: Paleomagnetic evidence from the Karmutsen Formation. *Canadian Journal of Earth Sciences, 17*, 1210–1228. https://doi.org/10.1139/e80-127

Zijderveld, J. D. A. (1967). A.C. Demagnetization of rocks: Analysis of results. *Developments in Solid Earth Geophysics, 3*, 254–286. https://doi.org/10.1016/B978-1-4832-2894-5.50049-5

Captions

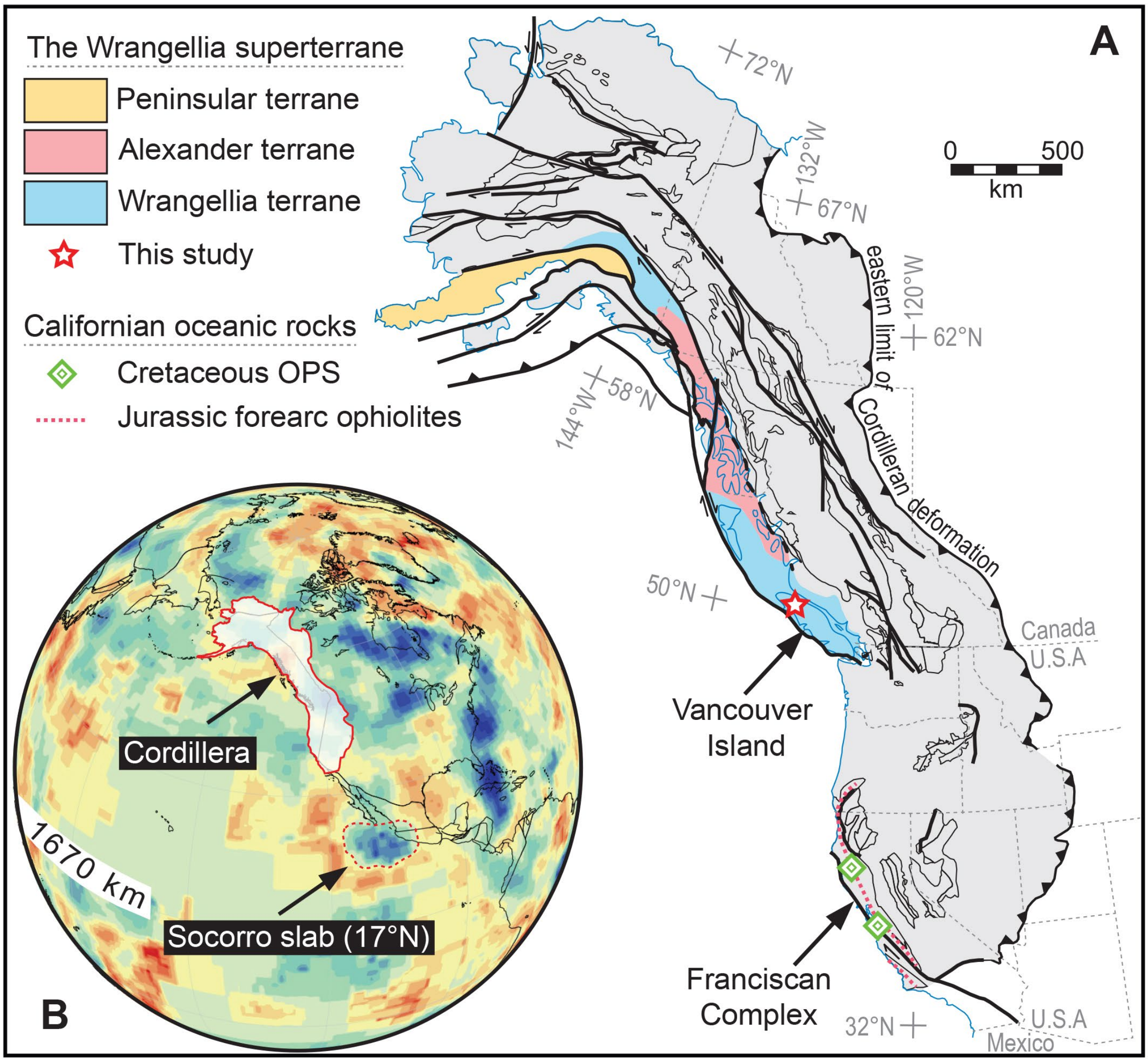

Figure 1. Tectonic setting of the Wrangellia superterrane and other geological records discussed in the text. (a) Tectonic map of the Cordillera of western North America (modified after Colpron & Nelson, 2009). (b) UUP07 P-wave tomographic model at 1670 km depth (Amaru, 2007) showing the location of the Socorro slab (offshore western Mexico) and the outline of the Cordillera of North America. Positive seismic wave-speed anomalies, such as the Socorro slab, are in blueish colors (up to +0.5%), whereas negative seismic wave-speed anomalies are in reddish colors (down to -0.5%).

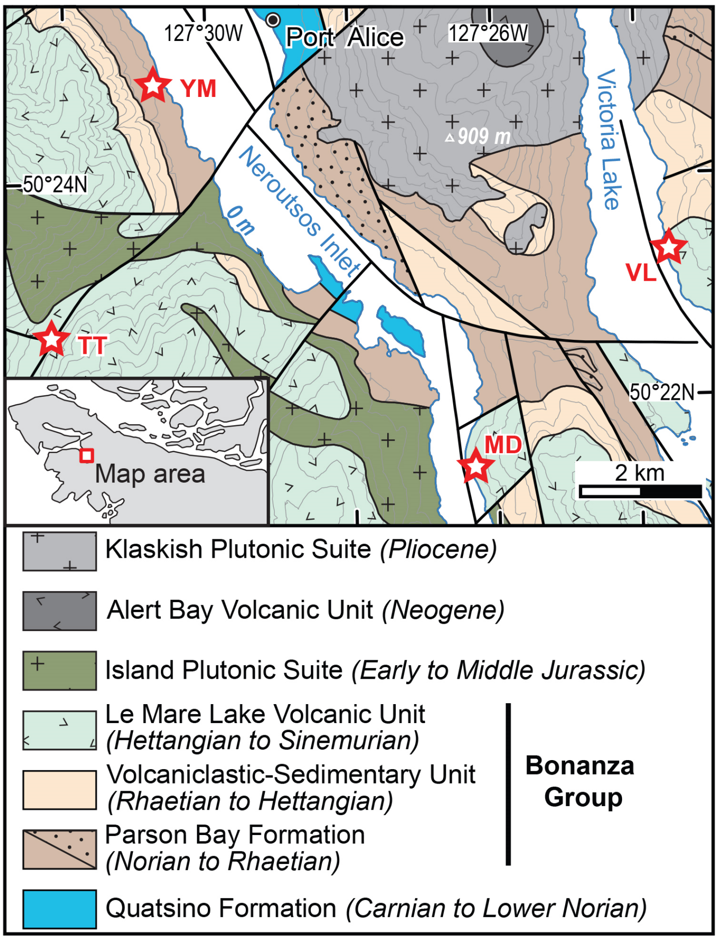

Figure 2. Geological map of the studied area in northern Vancouver Island (100 m contour interval; modified after Nixon et al., 2011a, 2011d), which is shown in the lower left inset. The red stars on the geological map indicate the four localities where paleomagnetic samples were collected. Localities VL-TT-MD are in the Le Mare Lake Volcanic Unit and locality YM is in the Parson Bay Formation. Parts of the Parson Bay Formation with higher volcaniclastic contents are indicated with a sandy lithological pattern.

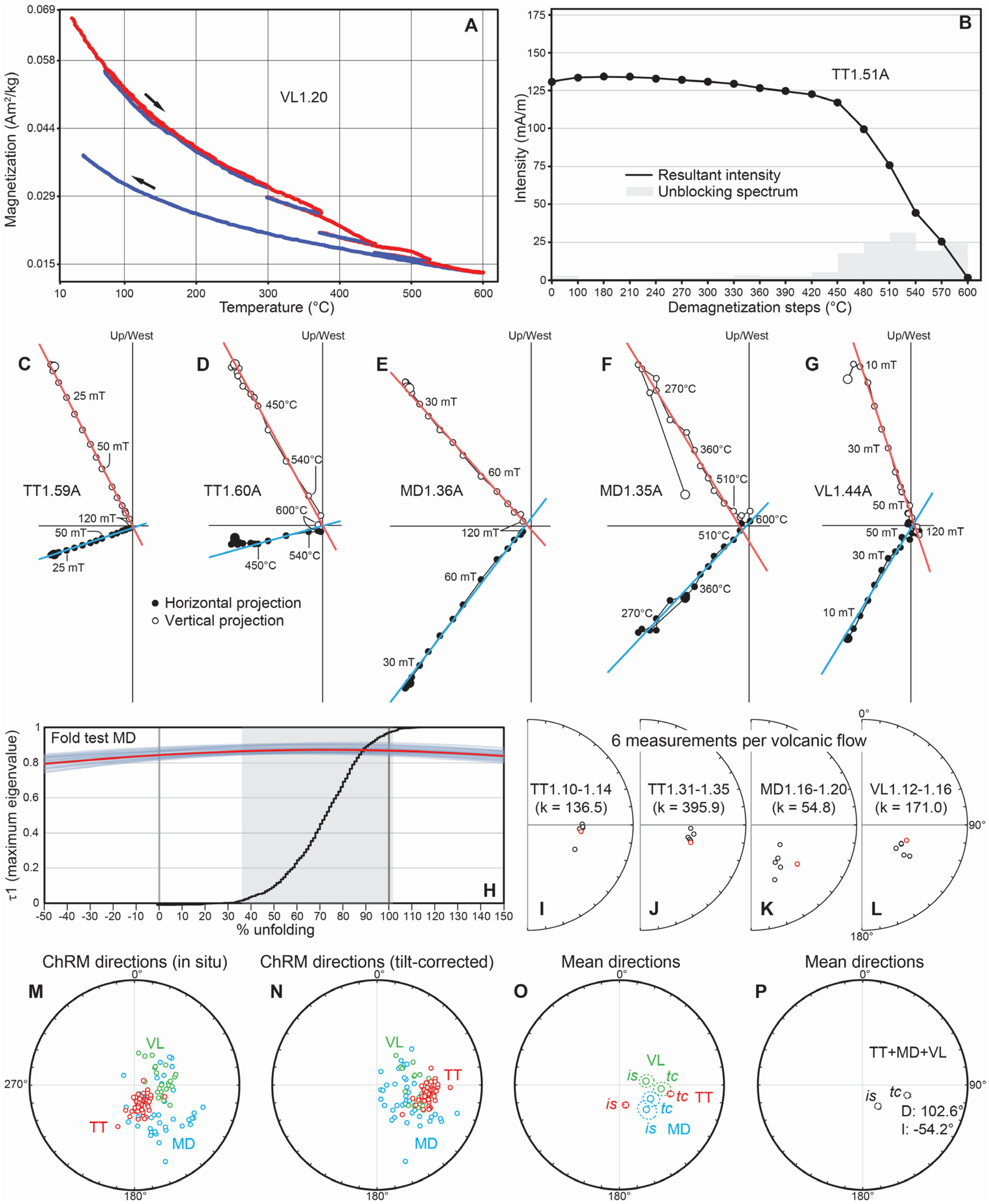

Figure 3. Rock magnetic and paleomagnetic results from volcanic localities TT, MD, and VL. (a) Thermomagnetic curves measured on a Curie balance. Heating segments are in red and cooling segments are in blue. (b) Intensity decay curve measured during TH treatment. (c)–(g) Orthogonal vector diagrams in geographic (= in situ) coordinates, where closed (open) symbols indicate declination (inclination). (h) Bootstrapped fold test of locality MD, with cumulative distribution function (confidence interval in light grey) based on 1000 bootstrap samples (mean

shown in red). (i)–(l) 6 characteristic remanent magnetization (ChRM) directions per volcanic flow in tectonic (= tilt-corrected) coordinates. For each flow, 5 directions from AF treatments (black circles) and 1 direction from TH treatment (red circle). k values correspond to the average (not shown) of the 6 directions. (m), (n) ChRM values from localities TT (red circles), MD (blue circles), and VL (green circles). (m) In situ coordinates. (n) Tilt-corrected coordinates. (o) Mean directions, including confidence intervals (dashed lines), of localities TT, MD, and VL. is = in situ coordinates, tc = tilt-corrected coordinates. (p) Same as in (o) with all localities combined. Declination and inclination values are for the tilt-corrected mean.

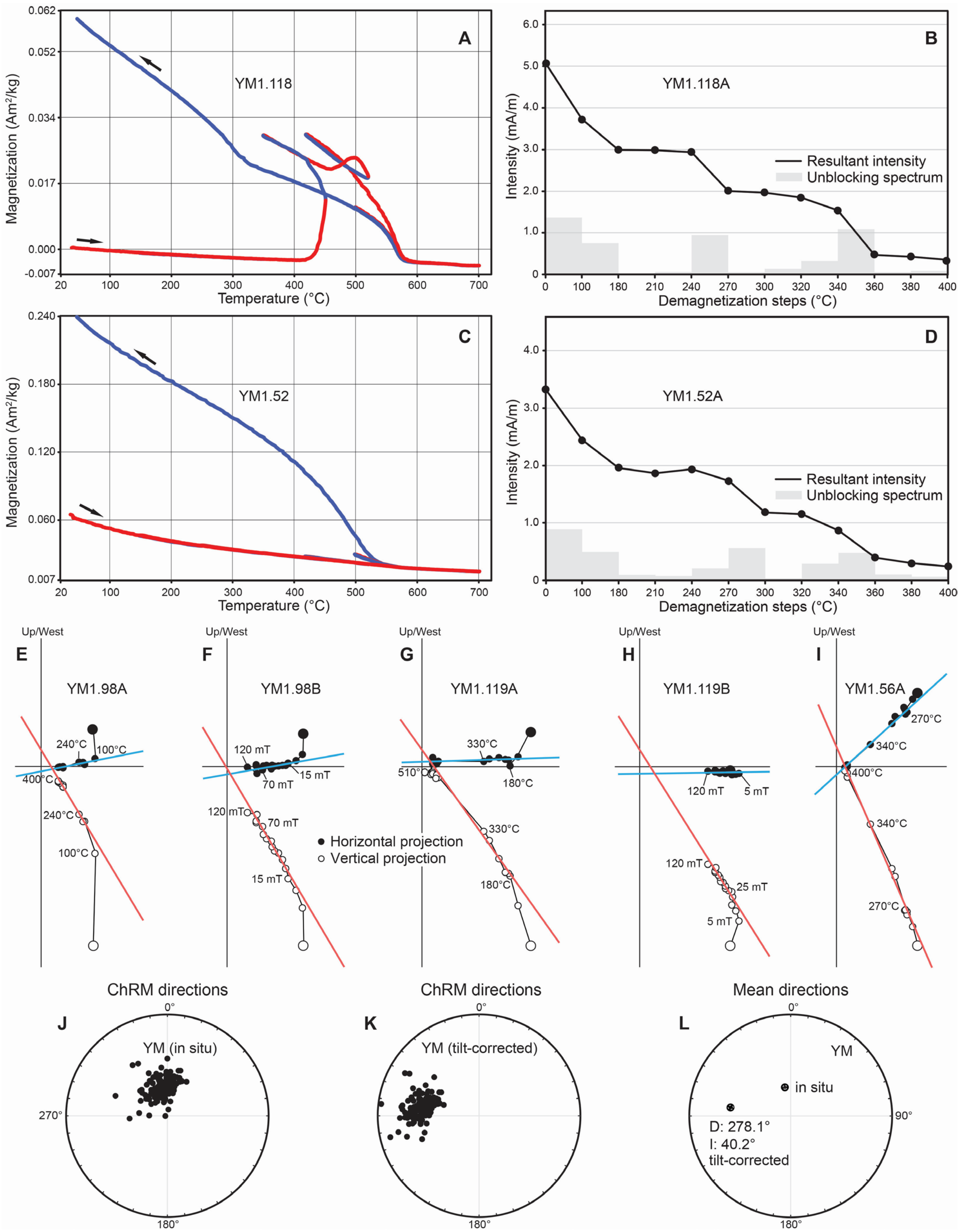

Figure 4. Rock magnetic and paleomagnetic results from sedimentary locality YM. (a), (c) Thermomagnetic curves measured on a Curie balance. Heating segments are in red and cooling segments are in blue. (b), (d) Intensity decay curves measured during TH treatment. (e)–(i) Orthogonal vector diagrams in geographic (= in situ) coordinates, where closed (open) symbols indicate declination (inclination). (j), (k) ChRM values from locality YM. (j) In situ

coordinates. (k) Tilt-corrected coordinates. (l) Mean directions, including confidence intervals (dashed lines), of locality YM. Declination and inclination values are for the tilt-corrected mean.

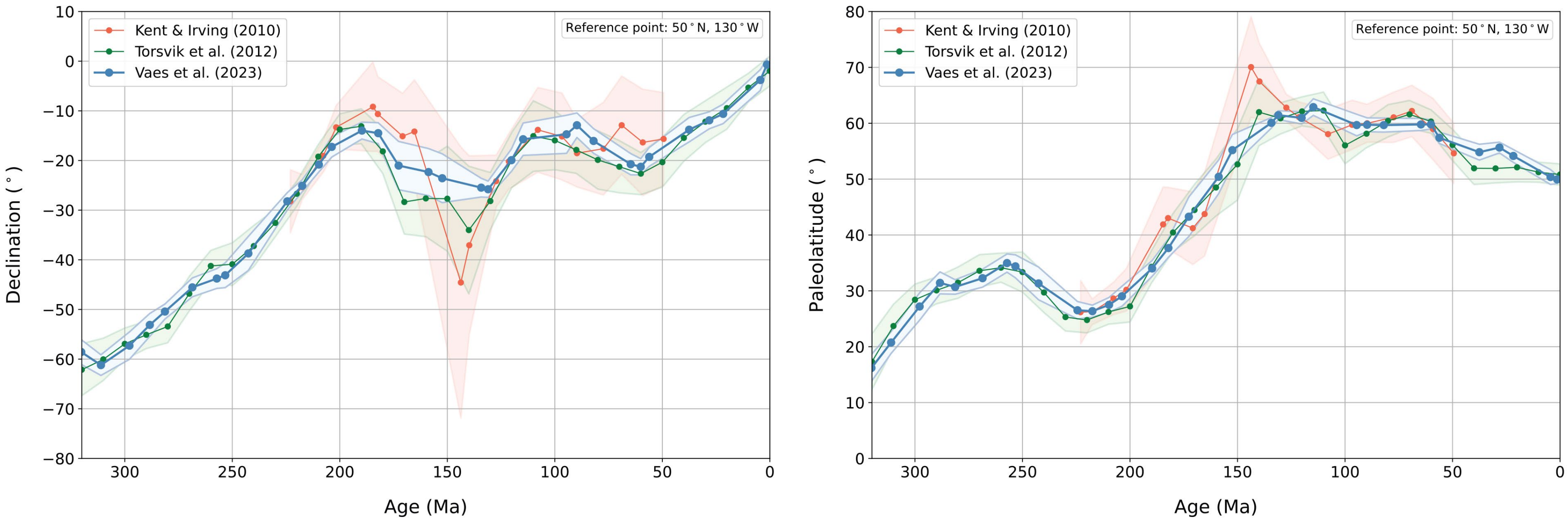

Figure 5. Declination and paleolatitude curves for the North American plate at a reference point at 50°N and 130°W, as predicted by three global APWPs. The colored bands show the 95% confidence regions for each curve. Note that the global APWP of Kent and Irving (2010) was computed for the 230 to 50 Ma time interval only.

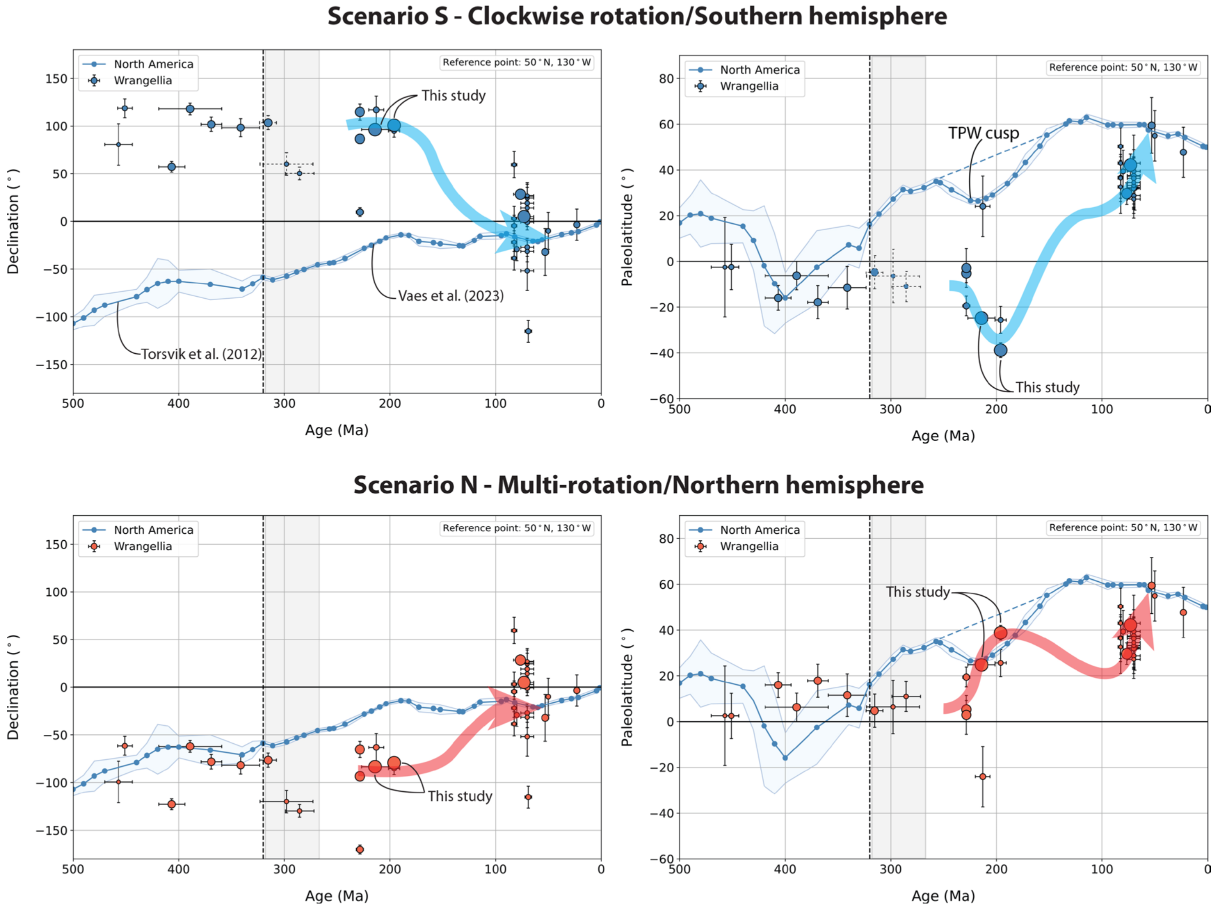

Figure 6. Paleomagnetic results obtained from the Wrangellia superterrane compared to predicted values for North America. Two possible scenarios are permitted by the hemispheric ambiguity of the pre-100 Ma paleomagnetic data: the upper panels show Scenario S (southern hemisphere) and the lower panels show Scenario N (northern hemisphere). Declination and paleolatitude values are computed for a reference point at 50°N and 130°W and are shown as blue or red dots with error bars indicating the age uncertainty and 95% confidence in the declination or paleolatitude. Predicted declination and paleolatitude curves–based on the global APWP of Vaes et al. (2023) for the last 320 Ma and North American APWP of Torsvik et al. (2012) for 320–500 Ma (transition marked by vertical dashed line)–are shown as blue curves (with 95% confidence region). The Carboniferous-Permian Kiaman superchron (~320–260 Ma) is indicated by the light grey band. The expected reversed polarity for the data from the superchron requires those plotted for Scenario S to be remagnetized (indicated by dashed error bars). The inferred effect of Triassic-Jurassic TPW on the paleolatitude of North America are highlighted. Paleomagnetic data are derived from the following sources (for numerical values, see Table 1 and Tables S1 and S2 in Data Set S3): Hillhouse (1977), Van der Voo et al. (1980),

Yole and Irving (1980), Panuska and Stone (1981), Hillhouse and Grommé (1984), Panuska (1985), Hillhouse et al. (1985), Irving & Yole (1987), Irving and Brandon (1990), Haeussler et al. (1992a, 1992b), Bazard et al. (1995), Butler et al. (1997), Grommé and Hillhouse (1997), Ward et al. (1997; E/I correction from Krijgsman & Tauxe, 2006), Enkin et al. (2001), Stamatakos et al. (2001), Kim and Kodama (2004; E/I correction from Krijgsman & Tauxe, 2006), and this study.

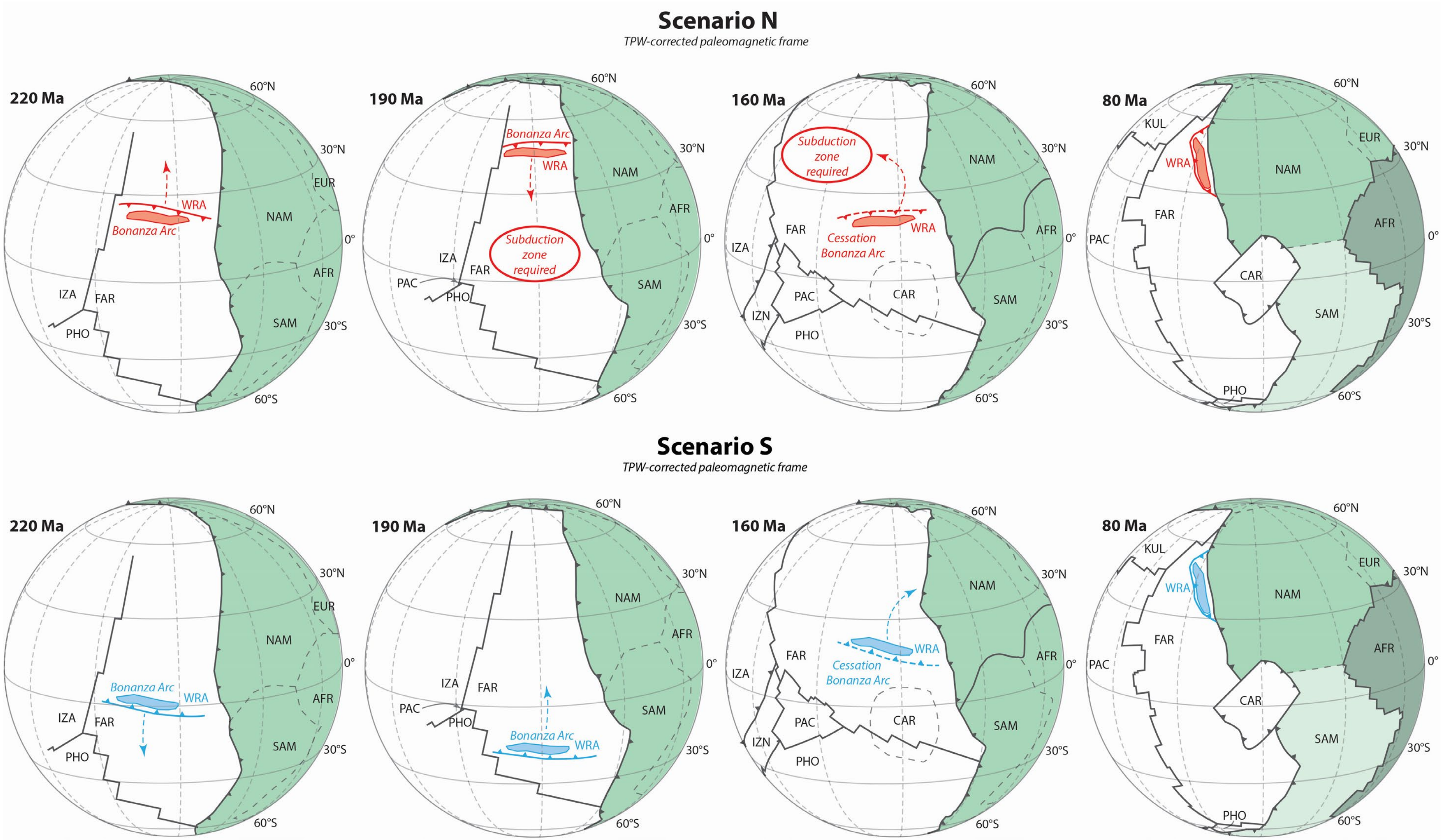

Figure 7. Schematic kinematic scenarios of the motion of the Wrangellia superterrane during the Late Triassic to Late Cretaceous (220 to 80 Ma). Scenario S shows a Late Triassic–Early Jurassic southward motion of ~15° followed by a northward motion of ~5000 km from the southern hemisphere accompanied by a clockwise rotation of ~110°. Scenario B depicts a rapid Late Triassic–Early Jurassic northward shift of ~20° in the northern hemisphere, followed by a southward motion of lower amplitude, and then a standstill at middle latitude accompanied by counterclockwise rotation of ~70°. AFR = Africa; CAR = Caribbean; EUR = Europe; FAR = Farallon; IZA = Izanagi; IZG = Izanami; KUL = Kula; NAM = North America; PAC = Pacific; PHO = Phoenix; SAM = South America; WRA = Wrangellia.

Table 1

Paleomagnetic Results of the Le Mare Lake Volcanic Unit (MD, VL, TT) and the Parson Bay Formation (YM)

						In situ				Tilt-corrected												
Locality	slat	slon	N	N45(is)	N45(tc)	D	ΔDx	I	ΔIx	D	ΔDx	I	ΔIx	k	α_{95}	K	A_{95Min}	A_{95}	A_{95Max}	λ	plat	plong
Le Mare Lake Volcanic Unit																						
MD	50.357	-127.439	41	n.a.	n.a.	132.2	13.0	-61.4	8.1	113.8	11.9	-63.2	6.8	13.7	6.3	8.1	2.7	8.4	7.9	-44.7	-47.3	346.7
VL	50.390	-127.392	24	n.a.	n.a.	81.5	13.5	-69.0	5.7	95.4	9.3	-56.9	7.0	32.9	5.2	17.2	3.4	7.4	11.1	-37.5	-31.1	346.3
TT	50.376	-127.546	58	n.a.	n.a.	161.3	6.3	-73.8	2.0	99.8	2.6	-48.7	2.6	98.0	1.9	70.4	2.4	2.2	6.4	-29.6	-28.7	335.7
MD-VL-TT	50.372	-127.480	123	108	117	142.9	6.8	-69.9	2.7	102.6	3.9	-54.2	3.2	29.1	2.5	17.9	1.8	3.2	4.1	-34.7	-35.0	340.8
Parson Bay Formation																						
YM	50.415	-127.512	138	n.a.	n.a.	347.0	3.95	66.7	1.9	278.1	1.8	40.2	2.3	48.7	1.7	52.7	1.7	1.7	3.7	22.9	23.0	151.9

Note. slat/slon = latitude and longitude of sampling location; N = total number of demagnetized samples; N45 = number of samples that fall within the 45° cutoff in in situ coordinates (is) and after tilt correction (tc); D, ΔDx = declination and associated error; I, ΔIx = Inclination and associated error; k and α_{95} = precision parameter and semiangle of the 95% cone of confidence around the computed site mean direction; K and A_{95} = precision parameter and semiangle of the 95% cone of confidence around the mean virtual geomagnetic pole; A_{95max} and A_{95min} = maximum and minimum value of A_{95} expected from paleosecular variation of the geomagnetic field; λ = paleolatitude of the locality; plat/plon = paleopole latitude and longitude; n.a. = not applicable.